Nonlinear Dyn (2024) 112:8299–8327
https://doi.org/10.1007/s11071-024-09497-9

ORIGINAL PAPER

Efficient numerical calculation of LYAPUNOV-exponents and stability assessment for quasi-periodic motions in nonlinear systems

Robert Fiedler · Hartmut Hetzler · Simon Bäuerle

Received: 9 March 2022 / Accepted: 4 February 2024 / Published online: 5 April 2024

Abstract Investigating the stability of stationary motions is a highly relevant aspect when characterizing dynamical systems. For equilibria and periodic motions, well established theories and approaches exist to assess their stability: in both cases stability may be assessed using eigenvalue analyses of small perturbations. When it comes to quasi-periodic motions, such eigenvalue analyses are not applicable, since these motions can not be parameterized on finite time intervals. However, quasi-periodic motions can be densely embedded on finite invariant manifolds with periodic boundaries. In this contribution, a new approach is presented, which exploits this embedding in order to derive a sequence of finite mappings. Based on these mappings, the spectrum of 1st order LYAPUNOV-exponents is efficiently calculated. If the linearization of the problem is regular in the sense of LYAPUNOV, these exponents may be used to assess stability of the investigated solution. Beyond the numerical calculation of LYAPUNOV-exponents, an approach is presented which allows to check LYAPUNOV-regularity numerically. Together, both methods allow for an efficient numerical stability assessment of quasi-periodic motions. To demonstrate, verify and validate the developed approach, it is applied to quasi-periodic motions of two coupled VAN- DER- POL oscillators as well as a quasi-periodically forced DUFFING equation. Additionally, a "step-by-step application instruction" is provided to increase comprehensibility and to discuss the required implementation steps in an applied context.

Keywords Quasi-periodicity · Hyper-time approach · Stability analyses · LYAPUNOV-exponents

1 Introduction and motivation

A quasi-periodic motion is a complex type of oscillation, which occurs in a variety of dynamical systems from academical to application oriented models. The theoretical fundamentals of quasi-periodicity are well understood and documented in the mathematical literature [8,41]. The key characteristic of quasi-periodic motions is that they can be embedded on invariant tori, which are invariant manifolds with periodic boundaries.

Concerning approaches to describe quasi-periodic motions, the majority aims at identifying the entire quasi-periodic invariant torus directly (*complete approximation*) or indirectly by describing sections (*invariant circle*). A variety of different approaches has been developed within the last decades [10,21,25,42,45] from which some were used to analyze nonlinear vibrations occurring in systems motivated by practical applications [18,19,36,44]. Most of the methods applied to dynamical systems with practical motivation are based on a *natural form* of the flow on quasi-periodic

R. Fiedler · H. Hetzler (✉) · S. Bäuerle
Institute for Mechanics, Engineering Dynamics Group, University of Kassel, Mönchebergstraße 7, 34125 Kassel, Germany
e-mail: hetzler@uni-kassel.de

invariant tori, which is also referred to as *hyper-time parametrization*.

Once a quasi-periodic invariant torus is identified, the embedding of the corresponding stationary quasi-periodic motion itself is known. However, the behavior of the flow in the immediate vicinity is still unknown and must be analyzed in order to assess the stability of the invariant solution.

LYAPUNOV-stability for equilibrium points and periodic motions is investigated by means of eigenvalues of the JACOBIAN and monodromy matrix, respectively. In both cases, the analyses of finite quantities (i.e., the system matrices) enable a statement concerning the asymptotic time behavior of a perturbation of the underlying solutions. If quasi-periodic motions are regarded, the identification of a finite quantity capturing the complete motion like the mentioned matrices is difficult, because unlike equilibria or periodic solutions a quasi-periodic solution does not exhibit characteristic segments of finite length in time (e.g., finite periods) on which stability assessments could be based on.

In order to assess the stability of quasi-periodic motions, different approaches have been described in the literature. In [41, Sect. 4.3], a criterion for the stability assessment of invariant tori is defined based on the distance between a trajectory and the torus. However, the direct application of this criterion to arbitrary systems exhibiting quasi-periodic motions relies on computing a LIPSCHITZ constant and an *index of exponential attraction*. It only makes a qualitative statement on stability.

The KAM (KOLMOGOROV- ARNOLD- MOSER) theory [2, Sect. 6.3] can be used for an analysis, if a quasi-periodic invariant torus of an unperturbed HAMILTONIAN-system persists under small perturbations. This approach is often applied in astrodynamics, since a description in terms of HAMILTONIAN-systems is valid in this context. In addition, a version for dissipative systems of the KAM-theory exists [9, App. B.3], [7]. Theoretically, the stability of quasi-periodic motions in dissipative systems can be assessed by this approach. However, the authors are not aware of an algorithmic implementation that can be used on general systems.

One of the first applicable methods for the stability characterization of quasi-periodic motions is introduced in [27–29]. This approach regards the eigenvalues of a higher order POINCARÉ-map at a fixed point, which represents a quasi-periodic motion of the underlying ODE. Because this method approaches quasi-periodic motions by means of a constant linear map of perturbations over the open time interval $t \in [0, \infty)$ (similar to a monodromy matrix), this criterion only enables a qualitative statement on the stability properties[1]

(cf. Subsect. 2.2). This qualitative stability assessment is often sufficient and is used in [12,23,30].

In [36,37], a method initially developed in [26] is utilized. The approach assumes a reducible invariant torus and is based on an approximation of eigenvalues of a FLOQUET-matrix to assess the stability of quasi-periodic motion. This approach is only used for HAMILTONIAN-systems, but the authors of [26] state that the approach can directly be applied to non-HAMILTONIAN ones. Similar to this contribution, the evolution of a perturbation is regarded within one pair of periodic boundaries of a quasi-periodic invariant manifold. However, an explicit formulation of the involved FLOQUET-matrix cannot be identified. Instead, eigenvalues of a related matrix, which is based on FOURIER-series approximation of the invariant boundary curve of the quasi-periodic motion, are investigated.

An alternative approach to the stability of a quasi-periodic motion based on the frequency domain representation is presented in [49]. The authors use a perturbed FOURIER-series approximation (also referred to as *perturbed harmonic balance*) and characterize the LYAPUNOV-exponents by singularities in the frequency-domain of the series.

In [33], the stability identification of quasi-periodic motions is also approached in the frequency domain. Here, a FOURIER-series is used to approximate the underlying quasi-periodic motion. A modeled perturbation is added by means of an exponentially varying (growing or decreasing) FOURIER-series. The stability is assessed by analyzing the variation rates, which coincide with the eigenvalues of the linearized problem. It is interesting to note, that this approach exhibits similarities to HILL's eigenvalue problem.

In this contribution, a systematic approach to the stability assessment of quasi-periodic motions in LYAPUNOV-regular systems by means of LYAPUNOV-exponents [5,34,35] is presented. In the following, the focus is set on the calculation of the LYA-

[1] Although stability is by definition a purely qualitative statement, quantitative measures such as eigenvalues for an equilibrium solution or FLOQUET multipliers for a periodic solution allow for a more comprehensive analysis (e.g., classification of bifurcations) and are therefore preferable results.

PUNOV-exponents and stability identification, while the preparatory step of calculating stationary quasi-periodic motions is only briefly addressed and their existence will be assumed.[2] In contrast to the applicable methods in the literature discussed above (e.g., [33,36,37,49]), the proposed method does not require a FOURIER-series approximation of the quasi-periodic invariant manifold. In fact, the method is independent of the way the invariant manifold was determined and has therefore a more general applicability.

The basic idea of the method is to use the embedding of a (infinite) quasi-periodic solution within a (finite) invariant manifold with periodic boundaries (torus). The periodic properties inherent to the torus representation allow for a systematic structuring of subsequent time intervals along the trajectory. Eventually, this allows to efficiently calculate long sequences of fundamental matrices, which map perturbations from boundary-to-boundary of the underlying quasi-periodic manifold.

This paper is organized as follows. In Sect. 2, a brief overview and discussion of some necessary fundamentals for the proposed approach are given. Subsequently, the stability identification approach is detailed in Sect. 3. In Sect. 4, the proposed approach is verified and validated by assessing the stability of quasi-periodic motions of two nonlinear dynamical systems, two coupled VAN- DER- POL oscillators and a quasi-periodically forced DUFFING equation. In order to facilitate the application of the presented approach, a "step-by-step instruction" is provided in Subsect. 4.1. Finally, a conclusion is given in Sect. 5.

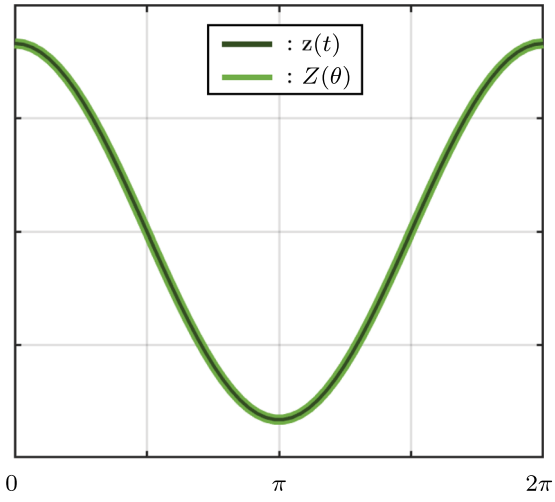

(a) Periodic motion

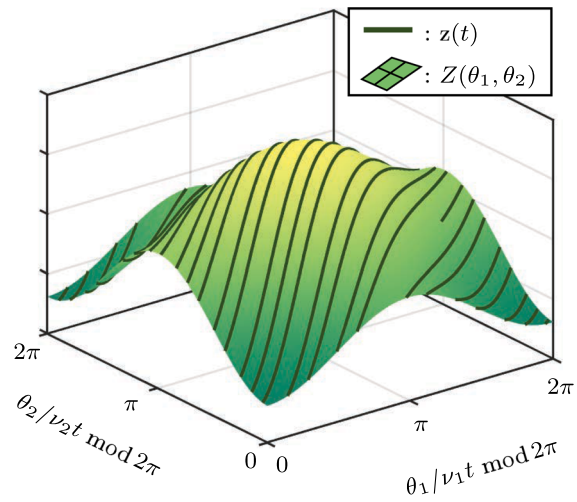

(b) Quasi-periodic motion

Fig. 1 Qualitative depiction of a torus function and a corresponding motion, both parameterized over hyper time $\boldsymbol{\theta} = \boldsymbol{\nu} t \mod 2\pi$

2 Introductory remarks on quasi-periodicity and LYAPUNOV-stability

Since the proposed stability identification method determines the LYAPUNOV-stability of quasi-periodic motions, some aspects concerning the theoretical fundamentals of the latter two are briefly discussed in this section.

2.1 Quasi-periodicity

Theoretical fundamentals of quasi-periodicity are comprehensively documented in the mathematical literature (cf. e.g., [8,41]). Moreover, some recent illustrative overviews and application oriented introductions can be found in [4,18]. In the following section, some basic concepts will be summarized as they will be fundamental for the derivation of the presented method.

[2] Details on this may be found in the corresponding literature surveyed above.

As a central characteristic, a quasi-periodic motion $\mathbf{z}_{\mathrm{qp}}(t) : t \mapsto \mathbb{R}^n$ in n-dimensional state space exhibits a frequency base $\boldsymbol{\nu} = [\nu_1, ..., \nu_p]$ of incommensurable (rationally independent) fundamental frequencies ν_i. Such a motion is embedded on a p-dimensional torus, which is the image of a *torus function* $\boldsymbol{Z}(\theta_1, \ldots, \theta_p) : \mathbb{T}^p \mapsto \mathbb{R}^n$. In this context, the parametrization $\boldsymbol{\theta} = [\theta_1, \ldots, \theta_p]$ of the torus function is often referred to as *torus coordinates*. The toroidal characteristic implies that the torus function exhibits periodic boundaries

$$\boldsymbol{Z}(..., \theta_i, ...) = \boldsymbol{Z}(..., \theta_i + 2\pi, ...), \quad i = 1, \ldots, p \tag{1}$$

and consequently describes a closed surface. Due to the incommensurability of the fundamental frequencies, the *quasi-periodic motion fills the torus function densely* [41]. Here, dense means that every point of the torus function $\boldsymbol{Z}$ is either identical or arbitrarily close to a point of the quasi-periodic motion trajectory $\mathbf{z}_{\mathrm{qp}}$. For *periodic* motions, which are a special case of quasi-periodic motions, the torus function is a one-dimensional object and it is also (trivially) filled by a corresponding trajectory (cf. Fig. 1a). Thus, for both cases, the longtime behavior of stationary solutions may conveniently be captured by investigating the invariant manifold on which they are embedded (cf. Fig. 1b).

Furthermore, from the property of density it can be concluded that torus functions are *invariant manifolds*. Assuming the trajectories exhibit asymptotic behavior, these invariant manifolds are attractors or repellors.

Yet, invariant manifolds in general describe a broader class of objects in state-space, where motions on them are not necessarily quasi-periodic. Therefore, a torus functions capturing a quasi-periodic motion is referred to as *quasi-periodic invariant manifold*.

A general, smooth dynamical system, which is formulated as a first order ordinary differential equation, is given by

$$\dot{\mathbf{z}} = \mathbf{f}(\mathbf{z}, t), \qquad \mathbf{f} : \mathbb{R}^n \times \mathbb{R} \mapsto \mathbb{R}^n. \tag{2}$$

Here, the explicit time dependence of the right-hand-side of Eq. (2) accounts for possible heteronomous influences like external forcing or explicitly prescribed variation of parameters. The right hand side is assumed to suffice a LIPSCHITZ-condition, which guarantees existence and uniqueness of solutions.

Assuming the externally imposed heteronomous influences are multi-harmonic with q base frequencies Ω_i $(i = 1, \ldots, q)$, the right hand side of Eq. (2) may be rewritten to

$$\dot{\mathbf{z}} = \mathbf{g}(\mathbf{z}, t), \qquad \mathbf{g} : \mathbb{R}^n \times \mathbb{R}^q \mapsto \mathbb{R}^n, \tag{3}$$

where

$$\begin{aligned} \mathbf{g}(\mathbf{z}, t) &= \mathbf{g}(\mathbf{z}, ..., \Omega_i t, ...) \\ &= \mathbf{g}(\mathbf{z}, ..., \Omega_i t + 2\pi, ...) \end{aligned} \quad i = 1, ..., q \tag{4}$$

holds. Moreover, it is assumed that Eq. (3) exhibits a general quasi-periodic solution $\mathbf{z}_{\mathrm{qp}}(t)$ with p fundamental frequencies $\boldsymbol{\nu} \in \mathbb{R}^p_+$. Consequently, the frequencies appearing in the system may be classified as follows:

- q *external base frequencies* Ω_i, which stem from external (heteronomous) influences such as forcing or imposed variation of parameters. These q frequencies are a priori known.
- $p-q$ *internal base frequencies* ω_j that are produced by internal (autonomous) mechanisms (i.e., *self-excitation*). These $p - q$ frequencies are unknown.

Thus, the frequency base $\boldsymbol{\nu}$ may be partitioned as

$$\boldsymbol{\nu} = [\boldsymbol{\Omega}, \boldsymbol{\omega}], \qquad \begin{matrix} \boldsymbol{\Omega} \in \mathbb{R}^q_+ \\ \boldsymbol{\omega} \in \mathbb{R}^{p-q}_+. \end{matrix} \tag{5}$$

A very popular choice of torus coordinates in application oriented investigations is the *hyper-time parametrization*, which relates torus coordinates and base frequencies by $\dot{\theta}_i = \nu_i$. Restricting these coordinates to a so-called coordinate torus $\mathbb{T} = [0, 2\pi)$ leads to

$$\theta_i = \nu_i t \mod 2\pi \quad with i = 1, \ldots, p. \tag{6}$$

In the mathematical literature, the latter connection between time t and the torus coordinates $\boldsymbol{\theta}$ is referred to as *natural form* (e.g., [42]) of the flow on the quasi-periodic invariant torus.

As a consequence of density of the flow on the manifold, Eq. (3) holds equally for the torus function in natural form

$$\frac{\mathrm{d}}{\mathrm{d}t}\boldsymbol{Z} = \mathbf{g}(\boldsymbol{Z}, t). \tag{7}$$

Expressing the explicit time dependency in Eq. (7) by using torus coordinates in substituting $\hat{\boldsymbol{\theta}} = \boldsymbol{\Omega} t \mod 2\pi$, the governing equation reads

$$\frac{\mathrm{d}}{\mathrm{d}t}\boldsymbol{Z} = \mathbf{g}(\boldsymbol{Z}, \hat{\boldsymbol{\theta}}), \qquad \mathbf{g} : \mathbb{R}^n \times \mathbb{T}^q \mapsto \mathbb{R}^n, \tag{8}$$

where $\hat{\boldsymbol{\theta}} = [\theta_1, \ldots, \theta_q]$. Now, considering again the relation $\boldsymbol{\theta} = \boldsymbol{\nu} t \mod 2\pi$, the time derivative can be

recast as

$$\begin{aligned}\frac{\mathrm{d}(.)}{\mathrm{d}t} &= \sum_{i=1}^{p} \frac{\partial(.)}{\partial\theta_i}\frac{\mathrm{d}\theta_i}{\mathrm{d}t} \\ &= \sum_{i=1}^{q} \frac{\partial(.)}{\partial\theta_i}\Omega_i + \sum_{i=q+1}^{p} \frac{\partial(.)}{\partial\theta_i}\omega_i .\end{aligned} \tag{9}$$

Summing all up, the fundamental equation to describe stationary quasi-periodic motions of the considered system by means of a torus function is obtained: this *invariance equation* reads

$$\sum_{i=1}^{q} \frac{\partial \boldsymbol{Z}}{\partial\theta_i}\Omega_i + \sum_{i=q+1}^{p} \frac{\partial \boldsymbol{Z}}{\partial\theta_i}\omega_i = \mathbf{g}(\boldsymbol{Z}, \hat{\boldsymbol{\theta}}). \tag{10}$$

The term *hyper-time parametrization* is derived from the fact that the solution of Eq. (10) is a torus function, which depends on multiple time scales $\boldsymbol{Z}(\theta_1, \ldots, \theta_p)$ with $\theta_i = \nu_i t \mod 2\pi$ for $i = 1, \ldots, p$ (e.g., [19]).

If a solution of Eq. (10) is sought, the system exhibits n equations for $n + p - q$ unknowns ($\boldsymbol{Z} : \mathbb{T}^p \mapsto \mathbb{R}^n$ and $\boldsymbol{\omega} \in \mathbb{R}^{p-q}$). In case of a purely external excitation ($q = p$), Eq. (10) is solvable, in case of the occurrence of self-excitation mechanism ($q < p$), $p-q$ additional equations are required to close the equation system, due to translational invariance. These additional equations are *phase conditions* for which different formulations exist. Due to good convergence properties, an integral formulation

$$\int_{\mathbb{T}^p} \boldsymbol{Z}^{\top} \frac{\partial \boldsymbol{Z}_0}{\partial\theta_i}\,\mathrm{d}\boldsymbol{\theta} = 0, \qquad i = q+1, \ldots, p \tag{11}$$

introduced in [42] is often used. In Eq. (11), $\boldsymbol{Z}_0$ represents a nearby torus function. It is noteworthy that $\boldsymbol{Z}_0$ does not have to be an exact solution of the considered problem, because its main purpose in Eq. (11) is to provide a reference to fix the parametrization of $\boldsymbol{Z}$ and thus overcome the translational invariance (cf. [42]).

By solving Eq. (10) and (11) with respect to $\boldsymbol{Z}$ and $\boldsymbol{\omega}$, the torus function is identified and the flow of the embedded quasi-periodic motion can be derived by Eq. (6). It is interesting to note that for periodic motions, which are parameterized over one-dimensional tori $\mathbb{T}^1$ (i.e., $p = 1$), Eq. (10) and (11) correspond to the classical problem formulation used in MATCONT [22] or AUTO [16]. Beyond this, for $p > 1$ Eq. (10) and (11) are able to capture multi-frequent, quasi-periodic oscillations.

Therefore, these equations offer a generalized approach to describe periodic as well as quasi-periodic motion in a common (hyper-) time-based framework.

The invariant manifold described by Eq. (10) and (11) can be discretized and solved by common methods such as the FOURIER- GALERKIN method [3,19,23], the Finite Difference method [18,42] or the Shooting Method [21,36].

An alternative approach to determine the torus function $\boldsymbol{Z}$ of Eq. (10) *indirectly*, aims on finding a periodic boundary hyper-plane of the torus function. Because Eq. (10) is a semi-linear PDE, the *method of characteristics* can be applied. As a result, the system of ordinary differential equations (ODEs)

$$\frac{\mathrm{d}\theta_i}{\mathrm{d}t} = \Omega_i \qquad i = 1, \ldots, q \tag{12a}$$

$$\frac{\mathrm{d}\theta_j}{\mathrm{d}t} = \omega_j \qquad j = q+1, \ldots, p \tag{12b}$$

$$\frac{\mathrm{d}\boldsymbol{Z}}{\mathrm{d}t} = \mathbf{g}(\boldsymbol{Z}(\boldsymbol{\theta}(t)), \hat{\boldsymbol{\theta}}(t)) \tag{12c}$$

is obtained, which describes the invariant manifold along characteristic lines. Here, the characteristic variable coincides with time t. In order to determine specific solutions of Eq. (12), initial conditions must be defined: since the characteristics in Eq. (12) may be seen as a continuous set of solutions which simultaneously start at a specified time (e.g., $t = 0$), these initial conditions must be a $(p-1)$-dimensional sub-manifold $\boldsymbol{Z}(t = 0) \stackrel{!}{=} \hat{\boldsymbol{Z}}$ of the p-dimensional solution to Eq. (10). In order to parameterize this manifold $\hat{\boldsymbol{Z}} = \hat{\boldsymbol{Z}}(\boldsymbol{\rho}) : \mathbb{T}^{p-1} \mapsto \mathbb{R}^n$ of initial conditions, $(p-1)$ coordinates according to

$$\boldsymbol{\rho} = [\rho_1, \ldots, \rho_{p-1}] = [\theta_2, \ldots, \theta_p] \tag{13}$$

may be introduced. Eventually, this parameterization corresponds to a sub-manifold $\hat{\boldsymbol{Z}} = \hat{\boldsymbol{Z}}(\boldsymbol{\rho})$ of initial conditions in the initial hyperplane at $\theta_1 = 0 = \text{const}$. By virtue of the periodicity properties of the underlying invariant solution, the chosen initial conditions will also be periodic according to

$$\begin{aligned}&\hat{\boldsymbol{Z}}(..., \rho_i, ...) = \hat{\boldsymbol{Z}}(..., \rho_i + 2\pi, ...), \\ &\quad i = 1, \ldots, p-1.\end{aligned} \tag{14}$$

As examples, the following typical cases may be distinguished:

- periodic solutions ($p = 1$): for one-dimensional invariant manifolds the initial sub-manifold $\hat{\boldsymbol{Z}} : \mathbb{T}^0 \mapsto \mathbb{R}^n$ is a single *point*.

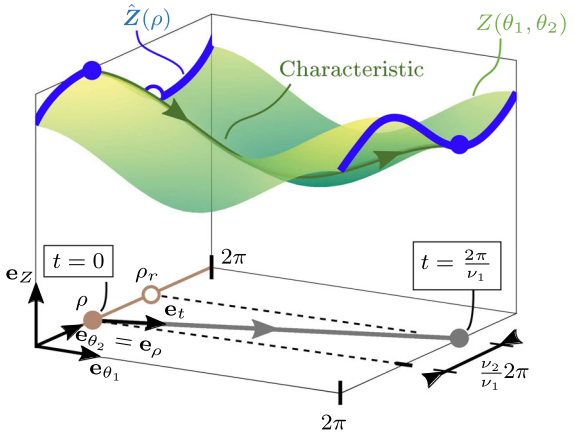

Fig. 2 Illustration of approximating a quasi-periodic motion ($p = 2$) by means of a periodic boundary hyper-plane $\hat{\boldsymbol{Z}}(\rho)$

- quasi-periodic solutions ($p = 2$): for two-dimensional invariant manifolds the initial manifold $\hat{\boldsymbol{Z}}(\rho) : \mathbb{T}^1 \mapsto \mathbb{R}^n$ is a *curve*. This particular case is shown in Fig. 2.

Because the characteristics—which are sections of the underlying quasi-periodic trajectory—evolve in a parallel flow (natural form),[3] the position on the coordinate torus, where a characteristic recurs to the periodic hyper-plane $\theta_1 = 0$, can be calculated as function of the frequencies. The characteristic time, which trajectories require to recur to the initial hyper-plane, is $t_r = \frac{2\pi}{\nu_1}$. Thus, a characteristic starting at $\boldsymbol{\rho}$ recurs at

$$\boldsymbol{\rho}_r = \frac{2\pi}{\nu_1}\hat{\boldsymbol{\nu}} + \boldsymbol{\rho} \mod 2\pi \tag{15}$$

where $\hat{\boldsymbol{\nu}} = [\nu_2, \ldots, \nu_p]$ (cf. Fig. 2). According to Eq. (14), initial sub-manifolds on the invariant manifold must be periodic from one initial hyperplane to the other. Thus, the equation

$$\hat{\boldsymbol{Z}}(\boldsymbol{\rho}_r) - \hat{\boldsymbol{Z}}(\boldsymbol{\rho}) = \mathbf{0} \tag{16}$$

has to be solved in order to determine $\hat{\boldsymbol{Z}}$, where Eq. (12) is used to find $\hat{\boldsymbol{Z}}(\boldsymbol{\rho}_r)$. Because Eq. (16) is generally not fulfilled by an initial guess, it is solved using a shooting-method [18,36,37] or a collocation-method [14] combined with a solver for nonlinear algebraic equations (e.g., NEWTON-solver).

Conclusively, it is interesting to note that in the case of a periodic motion for either the non-autonomous ($p = 1,\ q = 1$) or the autonomous ($p = 1,\ q = 0$) case, Eq. (12) is identical to Eq. (10), highlighting the equivalence of a periodic torus function $\boldsymbol{Z}(\theta) : \mathbb{T} \mapsto \mathbb{R}^n$ and a periodic trajectory $\mathbf{z}_\mathrm{p}(t) : \mathbb{R} \mapsto \mathbb{R}^n$(cf. Fig. 1).

The stability criterion presented in this contribution is independent of the method for solving Eq. (10) and (11). However, the approach by means of the initial hyper-plane combined with a shooting method exhibits some advantages, because the required fundamental matrices (cf. Sect. 3) are a byproduct of the involved nonlinear equation solver (e.g., NEWTON-solver).

2.2 LYAPUNOV-stability

The notion of *stability* in the sense of LYAPUNOV [24,34,35] is based on the time evolution of small deviations

$$\Delta\mathbf{z}(t) = \mathbf{z}(t) - \mathbf{z}_0(t) \qquad \in \mathbb{R}^n \tag{17}$$

between a perturbed solution $\mathbf{z}$ and the unperturbed reference solution $\mathbf{z}_0$ of Eq. (2) for general solutions or Eq. (3) for (quasi-)periodic solutions. Inserting the decomposition from Eq. (17) into Eq. (2) or Eq. (3) and subsequent TAYLOR-expansion about $\mathbf{z}_0(t)$ yields

$$\Delta\dot{\mathbf{z}}(t) = \boldsymbol{J}(t)\Delta\mathbf{z}(t) + \mathcal{O}(\Delta\mathbf{z}^2(t)), \tag{18}$$

where $\boldsymbol{J}(t) = \left[\partial g_i/\partial z_j\big|_{\mathbf{z}=\mathbf{z}_0}\right] \in \mathbb{R}^{n\times n}$ is the JACOBIAN-matrix along the reference solution $\mathbf{z}_0$.

LYAPUNOV*'s first or indirect method* assesses the stability of the reference $\mathbf{z}_0$ by evaluating the long-term temporal behavior of $\Delta\mathbf{z}(t)$ by the linearization

$$\Delta\dot{\mathbf{z}}(t) = \boldsymbol{J}(t)\Delta\mathbf{z}(t). \tag{19}$$

Here, the local behavior is of interest and perturbations may be assumed to be small ($\Delta\mathbf{z}(t) \ll 1$).

It can be proven that the resulting stability characteristics of Eq. (19) are equivalent to those of Eq. (18), if the linearization (19) is *regular* in the sense of LYAPUNOV [5,11,24,35]: the definition and further details are given below. In particular, PERRON-like effects are ruled out by this condition. Moreover, only cases can be decided where the investigated solution $\mathbf{z}_0(t)$ is *hyperbolic*.[4] Since Eq. (19) is a linear ODE, the solution can

[3] The parallel flow is a consequence of the chosen *hyper-time parametrization*.

[4] Roughly speaking, a solution is hyperbolic if perturbations in its *normal directions* exhibit either a contracting or an expanding behavior—the critical case of indifferent (neutral) behavior cannot be decided based on Eq. (19) (cf. [18, Sect. 4] and [31, Sect. 2.3]).

be written in explicit form as

$$\Delta\mathbf{z}(t) = \boldsymbol{\psi}(t,0)\Delta\mathbf{z}(0), \tag{20}$$

where $\boldsymbol{\psi}(t,0) \in \mathbb{R}^{n\times n}$ is the fundamental matrix, which maps an initial perturbation to the perturbation at time t. Since the right hand side of Eq. (3) is assumed to suffice a (local) LIPSCHITZ-condition the partial derivatives are bounded: thus, the norm[5] of $\boldsymbol{J}(t)$ satisfies

$$||\boldsymbol{J}(t)|| \leq C. \tag{21}$$

This implies that the growth of perturbations is exponentially bounded and thus the fundamental matrix satisfies

$$||\boldsymbol{\psi}(t,0)|| \leq K\mathrm{e}^{Ct}. \tag{22}$$

Depending on the type of solution and the corresponding time-dependency of $\mathbf{J}(t)$ in Eq. (19), the following cases can be distinguished:

- *equilibria* where $\mathbf{J} = \text{const}$: Here, the general fundamental matrix can be determined as $\boldsymbol{\psi}(t,0) = e^{\boldsymbol{J}t}$. Solutions will be asymptotically stable if all eigenvalues λ_i (i=1,…, n) of $\mathbf{J}$ have negative real parts.
- *periodic solutions* with $\mathbf{J}(T+t) = \mathbf{J}(t)$: For such solutions the stability can be assessed by investigating the eigenvalues/ FLOQUET multipliers Λ_i $(i = 1,\ldots,n)$ of the *monodromy matrix* $\boldsymbol{M} = \boldsymbol{\psi}(T+t,t) = \text{const}$, which is the fundamental matrix mapping a general state at t over the period T. Here, a solution will be asymptotically stable if the magnitudes of all $n-(p-q)$ (in general complex) FLOQUET multipliers Λ_i (i=1,…, n) of $\boldsymbol{M}$ are less than unity and $p-q$ multipliers are at most equal to unity.[6]
- *general stationary* solutions where $\mathbf{J}(t)$ exhibits some arbitrary time dependency: For such cases the stability of the reference $\mathbf{z}_0(t)$ may be judged by examining the (top) LYAPUNOV-exponent $\sigma_1 = \lim_{t\to\infty}\frac{1}{t}\ln||\boldsymbol{\psi}(t,0)\Delta\mathbf{z}(0)||$ or the LYAPUNOV-spectrum σ_i $(i = 1,\ldots,n)$. If the linearization in Eq. (19) is *regular*, non-chaotic stationary reference solutions $\mathbf{z}_0$ to Eq. (2) or Eq. (3) are asymptotically stable, if all $n-p$ LYAPUNOV-exponents σ_i are smaller than zero—the remaining p exponents are exactly zero and indicate the dimension of the invariant manifold (p-torus).[7]

Obviously, in all cases the fundamental matrix plays a central role. Subsequently, the approaches for periodic and general solutions are briefly summarized, since a combination of those two methods will be used to approach the stability of quasi-periodic solutions.

2.2.1 Periodic solutions

It can be proven that for periodic reference solutions the linearization in Eq. (19) is always *regular* in the sense of LYAPUNOV: thus, stability may be assessed using the linearization. For $\mathbf{z}_0(T+t) = \mathbf{z}_0(t)$ the constant *monodromy matrix* $\boldsymbol{M} = \boldsymbol{\psi}(T+t,t)$[8] maps perturbations from an arbitrary time t over one period T to $t+T$. Due to the periodicity of the investigated system,

$$\Delta\mathbf{z}(kT+t) = \boldsymbol{M}^k\Delta\mathbf{z}(t), \qquad \forall k\in\mathbb{Z} \tag{23}$$

holds. Based on Eq. (23), the stability of the periodic motion can be deduced from the eigenvalues of the monodromy matrix $\Lambda_i \in \mathbb{C},\ i = 1,\ldots,n$, which are called FLOQUET-multipliers. Moreover, it can be shown that

$$\Lambda_i = e^{\delta_i T}, \qquad \delta_i \in \mathbb{C},\ i = 1,\ldots,n \tag{24}$$

holds, where δ_i are called FLOQUET-exponents.

If a hyperbolic periodic motion stems from a *non-autonomous system* $\dot{\mathbf{z}} = \mathbf{g}(\mathbf{z},\Omega t)$—i.e., exhibiting a heteronomous frequency Ω—each FLOQUET-multiplier describes a contraction or expansion behavior normal to the periodic motion.

If the hyperbolic periodic motion occurs in an *autonomous system* $\dot{\mathbf{z}} = \mathbf{g}(\mathbf{z})$—i.e., exhibiting an autonomous frequency ω—one multiplier will be $\hat{\Lambda} = 1$, which indicates the "indifferent" behavior tangential to the periodic solution. The remaining multipliers describe contraction or expansion behavior in normal directions.

[5] Here, the 2-norm is used according to $||\boldsymbol{J}|| = \max||\boldsymbol{J}\mathbf{z}||/||\mathbf{z}|| = C$. From this follows $||\boldsymbol{J}\mathbf{z}|| \leq C||\mathbf{z}||$.

[6] For autonomous systems, there is always one FLOQUET multiplier exactly equal to unity. This multiplier describes the behavior of the perturbation into the tangential direction of the periodic limit cycle.

[7] Thus, the $p-n$ non-zero LYAPUNOV-exponents σ_i determine the behavior normal to the invariant manifold, while the p zero exponents belong to the indifferent behavior in the p-dimensional tangent space. For chaotic behavior, the attractor's dimension will no longer be an integer number and thus the relation between dimension and p will be more complicated.

[8] Obviously, this matrix is directly obtained from the fundamental matrix $\boldsymbol{\psi}$.

Defining $\Lambda_{n,i}$ as all FLOQUET-multipliers associated with the behavior normal to the solution, a periodic motion is considered asymptotically stable in the LYAPUNOV-sense if $|\Lambda_{n,i}| < 1,\ \forall i$ holds. If $\exists |\Lambda_{n,i}| > 1$, the periodic motion is unstable. For $|\Lambda_{n,i}| = 1$, the solution is non-hyperbolic and its stability may not be judged using linearized Eq. (19).

One further characteristic of this approach should be noted: the monodromy matrix $\boldsymbol{M}$ maps perturbations to a point $\mathbf{z}_0$ along the periodic solution over one period T. Thus, $\Delta\mathbf{z}(t)$ and $\Delta\mathbf{z}(T+t)$ exist in the same tangent space at $\mathbf{z}_0(t)$

$$\Delta\mathbf{z}(t),\ \ \Delta\mathbf{z}(T+t) \in \mathbb{R}^n_{\text{lin. } \mathbf{z}_0(t)}. \tag{25}$$

Consequently, the monodromy matrix is a *self-map*, by which an eigenvalue analysis can be used to deduce the stability. In contrast, fundamental matrices $\boldsymbol{\psi}(\tau, 0)$ at arbitrary times τ are no self-mappings, since they do not map between the same tangent spaces. Therefore:

- Tangential directions cannot be identified by $\lambda_i(\tau) = 1$, because the tangential space at $\mathbf{z}_0(0)$ is in general not equal to the tangential space at $\mathbf{z}_0(\tau)$
- For two arbitrarily chosen points in time $\hat{\tau} > \tau$, two eigenvalue sets $\lambda_i(\hat{\tau})$ and $\lambda_i(\tau)$ w.r.t. $\boldsymbol{\psi}(\hat{\tau}, 0)$ and $\boldsymbol{\psi}(\tau, 0)$ do not have to allow for an unambiguous conclusion on the stability behavior.

Consequently, such situations demand for different approaches.

2.2.2 *General non-chaotic stationary solutions and application to quasi-periodic solutions*

If the reference solution does not exhibit an obvious temporal structure, which could be exploited to analyze the fundamental matrix $\boldsymbol{\psi}(t, 0)$ (cf. Eq. (20)), a more general approach has to be chosen. For this purpose the generalized concept of LYAPUNOV-exponents is a common approach: originally devised by LYAPUNOV this concept [11,34,35] has been generalized to a broad class of ergodic dynamical systems by OSELEDEC [5, 38]. A recent comprehensive review can be found in [48].

For the special cases of stationary points or periodic motions the LYAPUNOV-exponents correspond to the real parts of the eigenvalues or the FLOQUET-multipliers, respectively.

LYAPUNOV-*Exponents:* Similar to eigenvalues or FLOQUET-multipliers, the concept of LYAPUNOV-exponents intents to quantify some sort of exponential growth rates of solutions. Therefore, the norm of the fundamental matrix must be bounded according to [48, p. 17]

$$\|\boldsymbol{\psi}(t, 0)\| \leq K \mathrm{e}^{ct} \quad , \forall t \geq 0. \tag{26}$$

Otherwise, measuring an exponential growth rate would not be appropriate to characterize the temporal behavior. For the systems under consideration, Eq. (26) is fulfilled since they are assumed to comply with a LIPSCHITZ condition and thus $\boldsymbol{J}$ is bounded (cf. Eq. (22)). From this follows finiteness according to

$$\limsup_{t\to\infty} \frac{1}{t} \ln \|\boldsymbol{\psi}(t, 0)\| < \infty\,. \tag{27}$$

Assume a perturbation $\Delta\mathbf{z}(t)$ evolving from the initial perturbation $\Delta\mathbf{z}(0) = \Delta\mathbf{z}_0$: then, the corresponding 1st order LYAPUNOV Characteristic Exponent is calculated as

$$\chi(\Delta\mathbf{z}_0) = \limsup_{t\to\infty} \frac{1}{t} \ln ||\Delta\mathbf{z}(t)|| \tag{28}$$

$$= \limsup_{t\to\infty} \frac{1}{t} \ln ||\boldsymbol{\psi}(t, 0)\Delta\mathbf{z}_0||. \tag{29}$$

Please note that under certain conditions lim sup may be replaced by lim: this will be discussed later in the context of regularity. Due to the assumption of exponential boundedness, finiteness of the LYAPUNOV-exponents given by Eq. (29) follows from Eq. (26) and Eq. (27).

Depending on the initial perturbation $\Delta\mathbf{z}_0 \in \mathbb{R}^n$, the resulting 1st order LYAPUNOV Characteristic Exponents $\chi(\Delta\mathbf{z}_0)$ can take up to n values[9] σ_i, which are typically arranged as ordered LYAPUNOV-spectrum

$$\sigma_1 \geq \sigma_2 \geq \cdots \geq \sigma_n, \tag{30}$$

where the σ_i are referred to as LYAPUNOV-exponents. Correspondingly,

$$\mathbb{L}_i = \left\{\Delta\mathbf{z}_0 \in \mathbb{R}^n \ \ , \ \chi\left(\Delta\mathbf{z}_0\right) \leq \sigma_i\right\} \quad i = 1, \ldots, n \tag{31}$$

defines n nested subspaces

$$\mathbb{L}_n \subset \cdots \subset \mathbb{L}_2 \subset \mathbb{L}_1 = \mathbb{R}^n \tag{32}$$

[9] Similar to eigenvalues, the values of 1st order LYAPUNOV-exponents may appear with multiplicities larger than one.

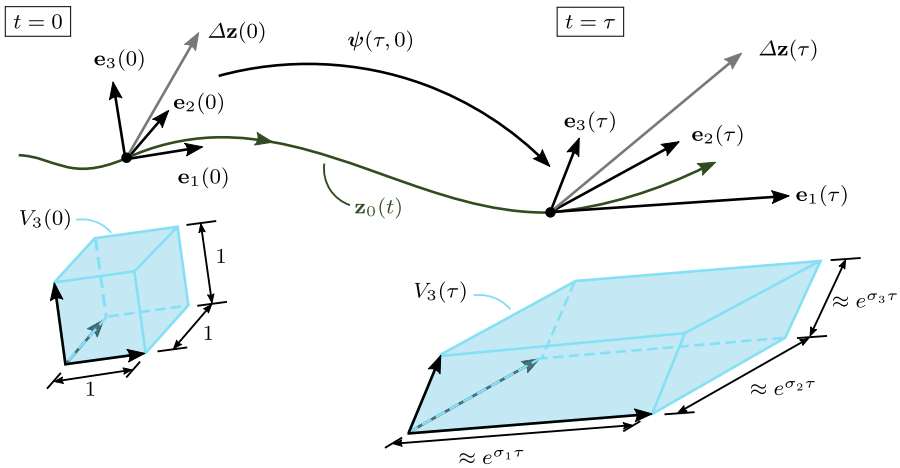

Fig. 3 Illustration of the behavior of the time dependent basis vectors $\mathbf{e}_i(t) : \mathbb{R} \mapsto \mathbb{R}^3$, the spectrum of 1st order LYAPUNOV-exponents σ_i and the volume V_3 for three dimensions at the initial time $t = 0$ and an arbitrary point in time $t = \tau$

of initial conditions, which are spanned by $\mathbf{e}_i(0)$ $(i = 1, \ldots, n)$ according to $\mathbb{L}_i = \text{span}\,(\mathbf{e}_n(0), \ldots, \mathbf{e}_i(0))$. Starting from $\mathbb{L}_n = \text{span}\,(\mathbf{e}_n(0))$ and iteratively adding new orthogonal base vectors to span subsequent subspaces, eventually the entire vector base $\{\mathbf{e}_i(0)\}$ $(i = 1, \ldots, n)$ can be chosen as an orthonormal system. Subjected to the dynamics of the system, these initial base vectors will evolve in time according to

$$\mathbf{e}_i(t) = \boldsymbol{\psi}(t, 0)\mathbf{e}_i(0) \tag{33}$$

and thus the perturbation may be represented as

$$\Delta\mathbf{z}(t) = \sum_{i=1}^{n} C_i \mathbf{e}_i(t), \qquad C_i \in \mathbb{R}. \tag{34}$$

In principle, all LYAPUNOV-exponents could be calculated using

$$\sigma_i = \chi\big(\mathbf{e}_i(0)\big) \quad i = 1, \ldots, n. \tag{35}$$

However, this approach is impractical since usually the bases $\mathbf{e}_i$ are not known in advance. Moreover, due to limited numerical precision *almost any* vector will have (sooner or later) components along $\mathbf{e}_1$ associated with the largest LYAPUNOV-exponent: therefore, in numerical calculations any starting vector will almost surely align with $\mathbf{e}_1$ and thus Eq. (29) will eventually yield the maximum exponent σ_1 (c.f. [5, p. 22]), since all other components decay faster or grow slower.

Note that Eq. (29) captures the long-term evolution of the norm $||\Delta\mathbf{z}(t)||$ of the initial perturbation *vector* (i.e., a 1D-volume). Alternatively, instead of considering such a single vector, the evolution of small m-dimensional subvolumes

$$V_m(t) = \text{vol}\big(\mathbf{e}_1(t), \ldots, \mathbf{e}_m(t)\big) = \mathbf{e}_1(t) \wedge \cdots \wedge \mathbf{e}_m(t) \tag{36}$$

of the tangent space can be regarded. If spanned by $m \leq n$ basis vectors $\{\mathbf{e}_i(t)\}$, $i = 1, \ldots, m$ they may be imagined as m-dimensional parallelepipeds (cf. Fig. 3). Note that for $m = n$

$$V_n(t) = \text{vol}\big(\mathbf{e}_1(t), \ldots, \mathbf{e}_n(t)\big) = |\det \boldsymbol{\psi}(t, 0)| \tag{37}$$

holds. By virtue of Eq. (27) $V_n(t)$ is finite. The corresponding mean temporal contraction or expansion rate of a sub-volume $V_m(t)$ is given by the mth order LYAPUNOV-exponent[10] (cf. Fig. 3)

$$\sigma^{(m)} = \chi(V_m) = \limsup_{t\to\infty} \frac{1}{t} \ln V_m(t). \tag{38}$$

LYAPUNOV- *Regularity:* In the context of LYAPUNOV-exponents the notion of LYAPUNOV-*regularity* plays an important role since it simplifies the calculations and allows assessing stability using LYAPUNOV-exponents.

Consider the linearization in Eq. (19) with corresponding LYAPUNOV-exponents

$$\sigma_1 \geq \sigma_2 \geq \cdots \geq \sigma_n. \tag{39}$$

The adjoint equation[11] to Eq. (19) reads

$$\dot{\mathbf{y}}(t) = -\boldsymbol{J}^\top(t)\mathbf{y}(t). \tag{40}$$

[10] Strictly speaking, also for mth order LYAPUNOV-exponents an entire spectrum exists. However, this is not important in the following and numerical calculations based on Eq. (38) will almost surely yield the largest exponent of this spectrum. Thus, *the* mth order LYAPUNOV-exponent will refer to the *largest* value of the corresponding spectrum, i.e., $\sigma^{(m)} = \sigma_1^{(m)}$.

[11] The adjoint equation follows from the constraint $\mathbf{y}^\top \Delta\mathbf{z} = \text{const}$.

Using the fundamental matrix $\boldsymbol{\psi}(t,0)$ to Eq. (19), the adjoint solution reads

$$\mathbf{y}(t) = \left[\boldsymbol{\psi}(t,0)\right]^{-\top} \mathbf{y}(0). \tag{41}$$

The corresponding (adjoint) LYAPUNOV-exponents are denoted by μ_i and ordered according to

$$\mu_1 \le \mu_2 \le \cdots \le \mu_n. \tag{42}$$

The linearization in Eq. (19) is called *regular*[12] if its LYAPUNOV-spectrum (cf. Eq. (39)) and the adjoint spectrum (cf. Eq. (42)) are mutually point symmetric according to (e.g., [11, § 67], [24, Ch. 64], [35, § 79])

$$\sigma_i = -\mu_i, \qquad i = 1, \ldots, n. \tag{43}$$

As a classical result, it can be shown that linearizations with constant or periodic Jacobians[13] are always regular. For the quasi-periodic case discussed here such a general result is unfortunately not available in literature.

However, in the authors' experience, regularity seems to be the norm rather than the exception in physics or engineering applications—this corresponds to the reportings of other authors (cf. for example [1,40]). Counterexamples to demonstrate the effects of non-regularity are usually specially designed [32,39] and seem not to be related to known physical problems in an obvious way.

However, one should be aware that using LYAPUNOV-exponents for stability assessments will only yield reliable results if regularity is guaranteed [11, §67], [24, Theorem 65.3 & 65.4], [35]. Consequently, regularity is a necessary prerequisite when investigating the stability of quasi-periodic motions.

LYAPUNOV-*exponents for regular systems:* In the following, regularity in the sense of LYAPUNOV is assumed. For regular problems, the limes involved in the calculation of the LYAPUNOV-exponents exist and thus "lim sup" in Eq. (29) and Eq. (38) may be replaced by "lim" [5], yielding the 1st and mth order exponents

$$\begin{aligned} \sigma &= \chi(\Delta\mathbf{z}_0) = \lim_{t\to\infty} \frac{1}{t} \ln ||\Delta\mathbf{z}(t)||, \\ \sigma^{(m)} &= \chi(V_m) = \lim_{t\to\infty} \frac{1}{t} \ln V_m(t). \end{aligned} \tag{44}$$

[12] Here, *regularity* refers to the definition by LYAPUNOV and is not related to the notion of regularity in the context of non-chaotic motion, smoothness of the dynamical system, or any of the numerous other definitions.

[13] Or, more general: *reducible* cases.

Both exponents are related by

$$\sigma^{(m)} = \sum_{i=1}^{m} \sigma_i^{(1)} = \sum_{i=1}^{m} \sigma_i, \qquad m = 1, \ldots, n. \tag{45}$$

Consequently, the full spectrum of 1st order LYAPUNOV-exponents of a regular system can be determined iteratively using

$$\begin{aligned} \sigma_1 &= \sigma^{(1)} \\ \sigma_m &= \sigma^{(m)} - \sigma^{(m-1)}, \qquad m = 2, \ldots, n. \end{aligned} \tag{46}$$

In order to calculate the sequence of mth order LYAPUNOV-exponents $\sigma^{(m)}$—and subsequently determine the spectrum of 1st order exponents σ_i – Eq. (38) could *in principle* be solved directly. One would subject an initially orthonormal basis $\{\mathbf{e}_i(0)\}$ $(i = 1, \ldots, m)$ to the linearized flow in Eq. (19) and thus analyze the evolution of an m-dimensional sub-volume $V_m(t)$ spanned by this basis.

Unfortunately, also in this context numerical calculations are influenced by the phenomenon that initially orthonormal basis vectors will align with the direction associated with the highest growth rate. Consequently, any initially finite sub-volume will shrink down to machine precision and, consequently, only the largest exponent could be identified in numerical calculations.

This problem can be circumvented by partitioning the time interval $[0, t]$ into k segments of length τ and expanding the volume $V_m(t)$ according to[14]

$$V_m(t) = \frac{V_m\big(k\tau\big)}{V_m\big((k-1)\tau\big)} \frac{V_m\big((k-1)\tau\big)}{V_m\big((k-2)\tau\big)} \cdots V(0). \tag{47}$$

Obviously, over the ith time segment $[(i-1)\,,\, i]\tau$ only the *ratio* $V_m\big((i)\tau\big)/V_m\big((i-1)\tau\big)$ is relevant. This allows for resetting the initial volume at the beginning of each sub-interval. A common method to do this is the *Discrete GRAM-SCHMIDT Orthonormalization* (DGSO) [5,6,47], by which the basis vectors are repeatedly re-orthogonalized after the preceding time-interval. This is done prior to calculating the evolution over the next interval and also includes a re-normalization of the basis vectors to avoid exponential growth of the vectors. Mainly this latter method is used within the proposed approach.

An alternative is the *Continuous GRAM-SCHMIDT Orthonormalization* (CGSO) [20]. Within this contribution, a modified version of CGSO according to [13] is

[14] For simplicity of notation it is assumed that $t = k\tau$.

used in Sect. 4.2 to validate the results obtained by the proposed method, which uses the DGSO.

Please note that methods involving re-orthogonalization and re-normalization like the DGSO and CGSO systematically avoid numerical overflows.

Beyond the above-mentioned general results, please be reminded of the following points, which are important in the context of quasi-periodic motions:

- The quasi-periodic trajectory is contained on an invariant compact manifold of the state space.
- As $t \to \infty$, *any* arbitrarily chosen quasi-periodic trajectory (i.e., independent of its initial conditions) will fill this invariant manifold densely. Thus, the entire motion is ergodic on this manifold.

Verifying regularity in numerical calculations: Using the relations summarized above in the context of stability, investigations rely on LYAPUNOV-regularity of the problem. In particular, regularity is important for the following crucial points:

- Replacing the "lim sup" by "lim".
- Using the mth order LYAPUNOV-exponent to determine the sum $\sigma^{(m)} = \sum_{i=1}^{m} \sigma_i$.
- Assessing stability using the LYAPUNOV-exponents.[15]

As mentioned before, for most applications in physics or engineering regularity can be assumed: up to the authors' knowledge, non-regular behavior has not been reported from experiments or simulations on physical problems and is usually associated with specially designed model problems. However, to guarantee reliable results, it may be desirable to check the regularity of the problem under consideration. For this purpose, we propose the following checks:

1. *Convergence towards* "lim": Check whether the involved expressions for $\sigma = \sigma^{(1)}$ and $\sigma^{(m)}$ really converge towards a limes. This will also help to verify whether the numerical calculation has converged or not. The existence of a limes is only a necessary condition, thus condition no. 2 must also be checked in order to prove regularity.
   In order to assess the convergence of the LYAPUNOV-exponents σ_i, the approximation s_i for finite time

$$s_i^{(m)}(t) := \frac{1}{t} \ln V_m(t) \tag{48}$$

of the mth order exponent[16] given by Eq. (38) is investigated with regard to its supremum and infimum by evaluating the difference

$$\Delta_{\lim}^{(m)} = \limsup_t s_i^{(m)}(t) - \liminf_t s_i^{(m)}(t). \tag{49}$$

If $\Delta_{\lim}^{(m)} = 0$ and if lim sup and lim inf converge towards stationary values, lim exists.
For the numerical evaluation, the time-continuous Eq. (48) for the exponents is evaluated at discrete time instants $t_k = k\tau$ on a finite time interval. Thus, for N_{map} time steps (mappings) this provides an equidistant discretization of the finite time interval $[0, N_{\text{map}}\tau]$. Eventually, for the resulting time-series $s_k^{(m)} = s^{(m)}(k\tau)$ $(k = 0, \ldots, N_{\text{map}})$ the relations to calculate the corresponding limes superior and limes inferior on the considered time interval read

$$\limsup_k s_k^{(m)} = \inf_{k\in\mathcal{K}} \sup_{\ell\in\mathcal{L}} s^{(m)}(\ell\tau) \tag{50}$$

$$\liminf_k \; s_k^{(m)} = \sup_{k\in\mathcal{K}} \inf_{\ell\in\mathcal{L}} \; s^{(m)}(\ell\tau) \tag{51}$$

where

$$\mathcal{K} = [0, 1, \ldots, (N_{\text{map}} - N_{\text{win}})] \tag{52}$$

$$\mathcal{L} = k, \ldots, N_{\text{map}}. \tag{53}$$

Here, the index k is not allowed to run through the entire time interval, but is restricted to $[0, (N_{\text{map}} - N_{\text{win}})]$ in order to guarantee that the $\sup_\ell$ in Eq. (50), as well as the $\inf_\ell$ in Eq. (51), apply to time series of a minimal window length N_{win} and thus may yield meaningful values.[17]
As a numerical indicator whether the "lim sup" and "lim inf" in Eq. (50), (51) converge onto each other—and thus whether the "lim sup" may be replaced by "lim"—one may monitor their difference as the length of the considered time interval increases.
To this end

$$\Delta_{\lim}^{(m)}(N_{\text{map}}, N_{\text{win}}) = \limsup_{k\in\mathcal{K}} \left\{ s_k^{(m)} \right\} - \liminf_{k\in\mathcal{K}} \left\{ s_k^{(m)} \right\} \tag{54}$$

[15] For non-regular systems, wrong results like the classical the PERRON-effect [32,39] could otherwise be obtained.

[16] For $m = 1$ this yields the first order exponent.

[17] If such a minimal window length was not applied at the end of $s_k^{(m)}$, for the last data point lim sup and lim inf would automatically coincide. In order to find appropriate values for N_{win}, different values should be studied.

quantifies the limit of the oscillation width of the sequence $s_k^{(m)}$ over the finite data sequence $k \in \mathcal{K} = [0, \ldots, (N_{\text{map}} - N_{\text{win}})]$.
If $\Delta_{\text{lim}}^{(m)}(N_{\text{map}}, N_{\text{win}}) \to 0$ as $N_{\text{map}} \to \infty$ this may serve as numerical indicator for equality of lim sup and lim inf and, thus, existence of lim, which implies regularity of the linearization.
For assessing the convergence of $\Delta_{\text{lim}}^{(m)}$ its dependence on N_{map} must be investigated for sufficiently large values of N_{map} and appropriate values of N_{win}. In this context it is recalled that LYAPUNOV-exponents typically exhibit convergence, which is hyperbolic over time.[18] Thus, it is recommended to observe the behavior of $\Delta_{\text{lim}}^{(m)}(N_{\text{map}})$ until hyperbolic (or faster) convergence is found.

2. *Regularity:* If convergence as necessary precondition is found, it should be checked whether the spectra of the system and its adjoint fulfill the condition in Eq. (43), i.e., if $\sigma_i + \mu_i = 0\,(i = 1, \ldots, n)$. This condition is necessary and sufficient for regularity. From an algorithmic point of view, this condition is in principle easy to verify: after calculating the LYAPUNOV-spectrum $\sigma_1 \geq \cdots \geq \sigma_n$ according to Eq. (39) of the original problem in Eq. (19), the spectrum $\mu_1 \leq \cdots \leq \mu_n$ (cf. Eq. (42)) of the adjoint problem in Eq. (40) is calculated. To this purpose, basically the same algorithm may be used as for the calculation of the spectrum σ_i (i=1,…, n). The only necessary modification is the usage of the fundamental matrix $\left[\boldsymbol{\psi}(t, 0)\right]^{-\top}$ of the adjoint system, which may directly be determined from the fundamental matrix of the original problem. Thus, no additional information or data will be necessary. Since the calculation of the adjoint spectrum basically follows the same algorithm, the numerical costs will roughly increase by the factor of two, plus the numerical costs of inversion of the fundamental matrix.
For the implementation, it will be necessary to account for numerical accuracy when determining σ_i and μ_i. Thus, it will be required to modify Eq. (43) to

$$|\sigma_i + \mu_i| \leq \epsilon_{\text{tol}} \quad , \qquad (i = 1, \ldots, n) \tag{55}$$

where ϵ_{tol} is a numerical tolerance parameter. Alternatively, one might consider monitoring the convergence of $|\sigma_i + \mu_i|$ simultaneous to the calculations. Please note that the regularity condition must be checked for all LYAPUNOV-exponents.

[18] In [15, p. 412] it is analytically shown that the error between a finite time estimate $\sigma_i(t)$ and the true limit σ_i converges $\sim \frac{1}{t}$.

3 An approach to calculate the LYAPUNOV-exponents and assess stability of quasi-periodic motions

A quasi-periodic motion can be interpreted as a type of motion, which lies between periodic and general motions: on the one hand—and unlike periodic motions—quasi-periodic motions cannot be described using a finite part of a trajectory. On the other hand, the representation as torus function reveals that a quasi-periodic motion exhibits strong structural characteristics—namely, periodicity with respect to the torus-coordinates. This strongly differs from unstructured general motions and may be utilized for further analyses. Moreover, quasi-periodic motions are non-chaotic.

First, it shall be emphasized that the standard approaches for periodic motions are unsuited to be applied to quasi-periodic motions. If the stability of a quasi-periodic motion was *approached like the one of a periodic motion*, the expression

$$\lim_{T_{qp} \to \infty} \Delta\mathbf{z}(T_{qp}) = \lim_{T_{qp} \to \infty} \boldsymbol{\psi}(T_{qp}, 0)\Delta\mathbf{z}(0) \tag{56}$$

would hold and $\boldsymbol{\psi}(T_{qp}, 0)$ would be a self-map. By that, the eigenvalues could be analyzed. However, even if such a self-map would exist from a rigorous mathematical point of view, only three types of eigenvalues would be identified due to the underlying linear problem (cf. Eq. (20)):

- $\Lambda_i = 0$: stable normal direction
- $\Lambda_i = 1$: tangential direction
- $\Lambda_i \to \infty$: unstable normal direction

If—in contrast to the latter—the stability of a quasi-periodic motion is *approached like the one of a general motion*, the spectrum of 1st order LYAPUNOV-exponents can be identified and the quantitative stability properties are characterized. However, this "brute force" approach would not make use of the additional information provided by the quasi-periodic invariant torus and the structure of the quasi-periodic trajectory embedded on it. Thus, it misses a potential increase in numerical efficiency.

In the following, an approach to identify the stability of quasi-periodic motions is derived, which combines the latter two approaches to overcome the drawbacks of each individual method. Therefore, two views on quasi-periodic motion are of importance: the representation as quasi-periodic time-trajectory $\mathbf{z}_{\mathrm{qp}}(t) : \mathbb{R} \mapsto \mathbb{R}^n$ as well as the representation as torus function $\boldsymbol{Z}(\boldsymbol{\theta}) : \mathbb{T}^p \mapsto \mathbb{R}^n$ (cf. Fig. 1).

Since Eq. (19) holds generally and the stability of a quasi-periodic motion is analyzed by means of the perturbation

$$\Delta \boldsymbol{Z}(\boldsymbol{\theta}) = \boldsymbol{Z}(\boldsymbol{\theta}) - \boldsymbol{Z}_0(\boldsymbol{\theta}), \tag{57}$$

the time derivative in Eq. (19) can be transformed with Eq. (9), by which

$$\sum_{i=1}^{q} \frac{\partial \Delta \boldsymbol{Z}(\boldsymbol{\theta})}{\partial \theta_i} \Omega_i + \sum_{i=q+1}^{p} \frac{\partial \Delta \boldsymbol{Z}(\boldsymbol{\theta})}{\partial \theta_i} \omega_i = \boldsymbol{J}(\boldsymbol{\theta}) \Delta \boldsymbol{Z}(\boldsymbol{\theta}) \tag{58}$$

results, where

$$\begin{aligned} &\boldsymbol{J}(..., \theta_i, ...) = \boldsymbol{J}(..., \theta_i + 2\pi, ...), \\ &\boldsymbol{J}(\boldsymbol{\theta}) : \mathbb{T}^p \mapsto \mathbb{R}^{n \times n} \end{aligned} \tag{59}$$

is the same JACOBIAN-matrix as in Eq. (19), but now parameterized over the torus coordinates $\boldsymbol{\theta}$. Although Eq. (58) is a PDE like Eq. (10), one should be aware that Eq. (58) *does not*—part from the trivial solution $\Delta \boldsymbol{Z}(\boldsymbol{\theta}) = \boldsymbol{0}$ (cf. Eq. (57))—exhibit a quasi-periodic invariant torus as solution if the underlying motion is hyperbolic. Recall that Eq. (58) describes the dynamical behavior of a perturbation $\Delta \boldsymbol{Z}(\boldsymbol{\theta})$.

Solving Eq. (58), the evolution of *one specific* perturbation can be analyzed. In order to capture the general behavior of perturbations, a fundamental matrix

$$\boldsymbol{\psi}(\boldsymbol{\theta}(t, t_0)) = [\Delta \boldsymbol{Z}_1(\boldsymbol{\theta}(t)), \ldots, \Delta \boldsymbol{Z}_n(\boldsymbol{\theta}(t))], \tag{60}$$

where t_0 is the initial time and $\Delta \boldsymbol{Z}_i(\boldsymbol{\theta}(t))\ i = 1, \ldots, n$ are linearly independent perturbations, can equivalently be regarded

$$\sum_{i=1}^{q} \frac{\partial \boldsymbol{\psi}(\boldsymbol{\theta})}{\partial \theta_i} \Omega_i + \sum_{i=q+1}^{p} \frac{\partial \boldsymbol{\psi}(\boldsymbol{\theta})}{\partial \theta_i} \omega_i = \boldsymbol{J}(\boldsymbol{\theta}) \boldsymbol{\psi}(\boldsymbol{\theta}) \tag{61}$$

since Eq. (58) is linear. Note that the fundamental matrix $\boldsymbol{\psi}(\boldsymbol{\theta}(t, t_0))$ describes perturbations of trajectories in the vicinity of the torus. Stated differently, it only holds *in time* and for a nearby trajectory (cf. Eq. (20)), but *not* for the *torus* itself.

Consequently, methods used to identify torus functions (periodic boundaries) are not applicable. However, since Eq. (61) is a linear PDE, its solution can be determined by the method of characteristics

$$\frac{\mathrm{d}\theta_i}{\mathrm{d}t} = \Omega_i \qquad i = 1, \ldots, q \tag{62a}$$

$$\frac{\mathrm{d}\theta_i}{\mathrm{d}t} = \omega_i \qquad i = q+1, \ldots, p \tag{62b}$$

$$\frac{\mathrm{d}\boldsymbol{\psi}}{\mathrm{d}t} = \boldsymbol{J}(\boldsymbol{\theta}(t)) \boldsymbol{\psi}(\boldsymbol{\theta}(t, t_0)), \tag{62c}$$

where the characteristic variable is just the time variable t of the ODE (cf. Eq. (2)).

Obviously, one could have directly written down Eq. (62) by simply taking Eq. (19). The authors refer the latter derivation as more descriptive and illustrative, because Eq. (62) emphasizes that the perturbation is a motion in the neighborhood of the toroidal reference surface.

In order to solve the ODE-system given by Eq. (62), a set of *initial hyper-values* $\hat{\boldsymbol{\psi}}(\boldsymbol{\rho})$ has to be defined, which is assumed to be continuously parameterized by the independent variables in the *parametrization vector* $\boldsymbol{\rho}$ (cf. Eq. (13)). This parametrization is chosen equivalently to the shooting approach for torus functions described in Sect. 2.1, namely

$$[\rho_1, \ldots, \rho_{p-1}] = [\theta_2, \ldots, \theta_p] \in \mathbb{T}^{p-1}, \tag{63}$$

by which a periodic boundary of the underlying torus function $\boldsymbol{Z}_0(\boldsymbol{\theta})$ is selected (cf. Fig. 4). It is important to note that for the following approach other parameterizations are equally acceptable, e.g.,

$$\begin{aligned} &[\rho_1, \ldots, \rho_{p-1}] = [\theta_1, \ldots, \theta_{i-1}, \theta_{i+1}, ...\theta_p], \\ &i \in [1, p], \end{aligned} \tag{64}$$

because different choices will only affect the integration time of the ODE (cf. Eq. (62)). Furthermore, by this choice of the initial hyper-plane parametrization, the transversality condition

$$\left| \frac{\partial \boldsymbol{\theta}}{\partial [t, \boldsymbol{\rho}]} \right| \neq 0, \tag{65}$$

required for the method of characteristics, is automatically fulfilled due to $\boldsymbol{\theta} = \boldsymbol{\nu} t \mod 2\pi$.

According to $\hat{\boldsymbol{\psi}}(\boldsymbol{\rho}) = \boldsymbol{I}$, the initial values are chosen constant where $\boldsymbol{I} \in \mathbb{R}^{n \times n}$ is the identity matrix. This choice gives rise to the following advantages:

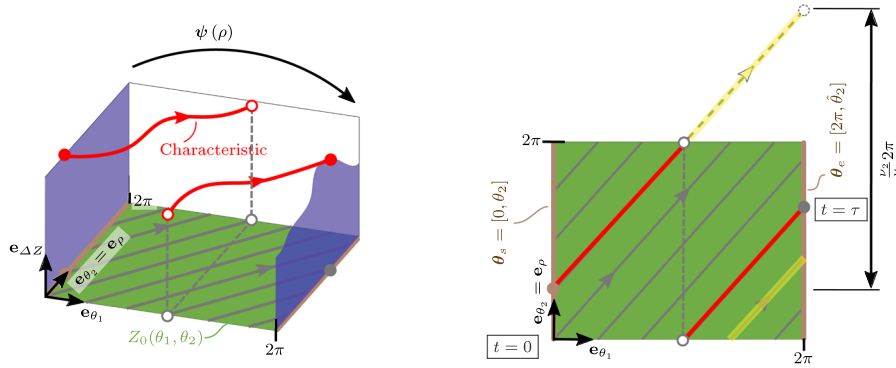

Fig. 4 Illustration of the mechanisms for mapping (unit) perturbations with the fundamental matrix function $\boldsymbol{\psi}(\rho)$ (left graphic) and parametrization details (right graphic) for two torus coordinates θ_1 and θ_2 ($p = 2$)

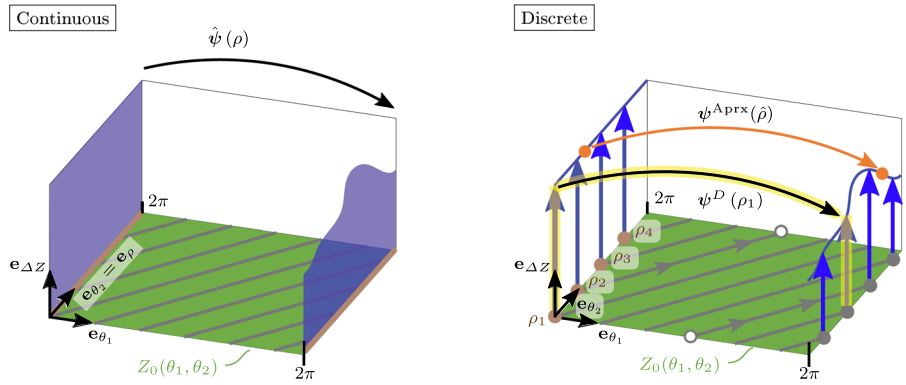

Fig. 5 Illustration of a mapping by the continuous fundamental matrix function $\hat{\boldsymbol{\psi}}(\rho)$, a mapping of a perturbation at supporting point ρ_1 by the corresponding discrete fundamental matrix $\boldsymbol{\psi}^D(\rho_1)$ and a mapping of a perturbation at an arbitrary point ρ by the interpolated fundamental matrix function $\boldsymbol{\psi}^{\mathrm{Aprx}}(\rho)$

1. Choosing a constant value, ensures periodic boundaries for the initial hyper-plane $\hat{\boldsymbol{\psi}}(\boldsymbol{\rho})$

$$\hat{\boldsymbol{\psi}}(..., \rho_i, ...) = \hat{\boldsymbol{\psi}}(..., \rho_i + 2\pi, ...) \quad i = 1, \ldots, p-1. \tag{66}$$

2. Choosing the identity matrix $\boldsymbol{I}$ as initial value and solving Eq. (62) provides a *normalized fundamental matrix function*, with which perturbations can directly be mapped (cf. Eq. (20)).

Having defined initial values, Eq. (62) can be solved by using a time integration scheme. The integration interval is chosen to be $t \in [0, \tau]$, where τ is the time a trajectory requires to recur to the initial hyper-plane (cf. Fig. 4). Due to the parallel flow on the torus function (cf. Eqs. (62a) and 62b), the recurrence time and the position on the parametrization of the initial values can be identified

$$\tau = \frac{2\pi}{\nu_1} \quad \text{and} \quad \theta_{e,i} = \frac{\nu_i}{\nu_1} 2\pi + \theta_{s,i} \mod 2\pi, \tag{67a}$$

$$\boldsymbol{\theta}_e = [0, \theta_{e,2}, \ldots, \theta_{e,i}, \ldots, \theta_{e,p}]^\top \tag{67b}$$

$$\boldsymbol{\theta}_s = [2\pi, \theta_{s,2}, \ldots, \theta_{s,i}, \ldots, \theta_{s,p}]^\top \tag{67c}$$

where $i = 2, \ldots, p$ and thus

$$\boldsymbol{\theta}_e = \boldsymbol{\gamma}(\boldsymbol{\theta}_s). \tag{68}$$

This relates the torus coordinates at *Poincaré* sections w.r.t. the underlying periodicities of the torus coordinates. Note that the latter relations correspond to the choice taken in Eq. (63). The solution of Eq. (62) with the stated parametrization and initial values is a fundamental matrix function $\boldsymbol{\psi}(\boldsymbol{\theta}_e, \boldsymbol{\theta}_s) : \mathbb{T}^p \mapsto \mathbb{R}^{n \times n}$, which maps an arbitrary perturbation over a periodic boundary of the torus function

$$\Delta \boldsymbol{Z}(\boldsymbol{\theta}_e) = \boldsymbol{\psi}(\boldsymbol{\theta}_e, \boldsymbol{\theta}_s) \Delta \boldsymbol{Z}(\boldsymbol{\theta}_s), \tag{69}$$

where $\boldsymbol{\theta}_e = \boldsymbol{\gamma}(\boldsymbol{\theta}_s)$. It is important to note that Eq. (69) is *only valid along the characteristics*.

Considering Eq. (69) and comparing this fundamental matrix function $\boldsymbol{\psi}(\boldsymbol{\theta}_e, \boldsymbol{\theta}_s)$ to the classical monodromy matrix $\boldsymbol{M} = \boldsymbol{\psi}(T + t, t)$ reveals that both map a perturbation over periodic boundaries. The crucial difference is that the monodromy matrix is a constant matrix which maps perturbations

$$\Delta \mathbf{z}(t), \ \Delta \mathbf{z}(T + t) \in \mathbb{R}^n_{\text{lin. } \mathbf{z}_0(t)} \tag{70}$$

within *the same linearized space*, which is the tangent space to the considered reference solution at equidis-

tant points in time. In contrast, the fundamental matrix function maps perturbations

$$\begin{aligned}\Delta\boldsymbol{Z}(\boldsymbol{\theta}_s) &\in \mathbb{R}^n_{\text{lin. } \boldsymbol{Z}_0(\boldsymbol{\theta}_s)}\\ \Delta\boldsymbol{Z}(\boldsymbol{\theta}_e) &\in \mathbb{R}^n_{\text{lin. } \boldsymbol{Z}_0(\boldsymbol{\theta}_e)}\end{aligned} \tag{71}$$

between *different tangential spaces* at $\boldsymbol{\theta}_e$ and $\boldsymbol{\theta}_s$, which relates the torus coordinates at *Poincaré*-sections on the coordinate torus that are at a distance of 2π.

Consequently, the fundamental matrix function is *not a self-map* and an eigenvalue analysis cannot be used to deduce the stability behavior (cf. Sect. 2.2—paragraph "periodic solutions"). Nevertheless, the identified fundamental matrix function $\boldsymbol{\psi}(\boldsymbol{\theta}_e, \boldsymbol{\theta}_s)$ enables the complete description of a perturbation $\Delta\boldsymbol{Z}(\boldsymbol{\theta})$ along the characteristics of the perturbation manifold Eq. (58) from border to border, which is known and can be evaluated for any arbitrary mapping.

According to Eq. (46), the spectrum of 1st order LYAPUNOV-exponents can be determined by calculating the mth order LYAPUNOV-exponents. In order to incorporate the idea of mappings from border to border into the definition of $\sigma^{(m)}$, the time t is divided in segments of length τ as given by Eq. (67a), and Eq. (47) is incorporated in Eq. (38). Eventually, this yields

$$\sigma^{(m)} = \lim_{k\to\infty} \frac{1}{k\tau} \sum_{i=1}^{k} \ln \frac{V_{m,i}}{V_{m,i-1}}, \tag{72}$$

where $V_{m,i}$ are m-dimensional subvolumes according to Eq. (36) at the time instances $\tau_i = i\tau$ at the end of the ith interval. To determine the sequence of $V_{m,i} = V_m(i\tau)$, m-dimensional hyper-cubes (cf. Eq. (36)) are mapped over the periodic boundaries from the starting point $\boldsymbol{\theta}_s^{(i)} = \boldsymbol{\theta}_s(i\tau)$ to the corresponding end point $\boldsymbol{\theta}_e^{(i)} = \boldsymbol{\gamma}(\boldsymbol{\theta}_s^{(i)})$. Evaluation of the fundamental matrix for these start and end points yields the mapping

$$\boldsymbol{\psi}^{(i)} = \boldsymbol{\psi}\left(\boldsymbol{\gamma}(\boldsymbol{\theta}_s^{(i)}), \boldsymbol{\theta}_s^{(i)}\right). \tag{73}$$

Obviously, these mappings are *not constant* matrices, but will depend on $\boldsymbol{\theta}_s$. However, they may be *efficiently handled* since the corresponding matrix function $\boldsymbol{\psi}(\boldsymbol{\theta}_s)$ can be numerically calculated a priori.

Next, the evolution of an m-dimensional hyper-cube (cf. Eq. (36)) over the ith interval is determined by investigating the evolution of small parallelepipeds given by

$$\begin{aligned}\Big[\mathbf{e}_1(i\tau), \ldots, \mathbf{e}_m(i\tau)\Big] = \boldsymbol{\psi}^{(i)}\Big[\hat{\mathbf{e}}_1\big((i-1)\tau\big), \ldots,\\ \hat{\mathbf{e}}_m\big((i-1)\tau\big)\Big].\end{aligned} \tag{74}$$

Here, $\left[\hat{\mathbf{e}}_1\big((i-1)\tau\big), \ldots, \hat{\mathbf{e}}_m\big((i-1)\tau\big)\right]$ is the re-orthonormalized vector bases after the preceding $(i-1)$th iteration and $\left[\mathbf{e}_1(i\tau), \ldots, \mathbf{e}_m(i\tau)\right]^{(i)}$ spans the parallelepiped at the end of the current ith iteration. From this latter one, the volume after the current mapping is calculated as $V_{m,i}(\tau) = \text{vol}\big(\mathbf{e}_1(i\tau), \ldots, \mathbf{e}_m(i\tau)\big)$.

After each iteration, a GRAM- SCHMIDT-orthonormalization is applied, which yields the re-orthonormalized basis $\left[\hat{\mathbf{e}}_1, \ldots, \hat{\mathbf{e}}_m\right]$ from the calculated basis $\left[\mathbf{e}_1, \ldots, \mathbf{e}_m\right]$. This step compensates for re-alignment of to the base vectors (orthogonalization) and accounts for the exponential growth or decay of the linearized system of perturbations (rescaling by normalization). In particular, the normalization step assures finiteness of perturbations and thus allows using the approach for stable as well as for unstable solutions over infinite time. Thus, the process can be executed arbitrarily often, which—eventually—means nothing else than executing an arbitrary sequence of the mappings according to Eq. (74).

Consequently, Eq. (72) may be evaluated for arbitrary large values of k until convergence is obtained.

In this context the question arises how long calculations must be carried out in order to obtain sufficient convergence. One possible approach is to apply moving average filtering and observe the oscillation width over a sliding time window of certain width. For the presented approach it is possible to efficiently adapt this strategy: if the LYAPUNOV-exponents of a p-torus for $p > 1$ are calculated, at least p exponents must be zero: thus, the corresponding true (converged) value is a priori known and the deviation can easily be determined as a measure of convergence.[19]

However, in a post-processing step, the convergence of all LYAPUNOV-exponents should be ensured.

Concerning the evaluation of the fundamental matrix function, it is interesting to note that due to incommensurability, the characteristics recur densely on the periodic boundary: thus, it will be necessary to evaluate the fundamental matrix function $\boldsymbol{\psi}\left(\boldsymbol{\gamma}(\boldsymbol{\theta}_s), \boldsymbol{\theta}_s\right)$ at arbitrary boundary points $\boldsymbol{\theta}_s$. To implement this within a numerical scheme, an interpolation approach may be

[19] Please note that this usually only refers to LYAPUNOV-exponents along the tangential direction of the torus corresponding to an autonomous base frequency—exponents and their tangential directions associated with non-autonomous frequencies are externally prescribed and thus imposing perturbations is usually not meaningful.

used. *First*, a finite number N_{Ch} of characteristics is determined and the corresponding fundamental matrices are calculated:

$$\begin{aligned} &\boldsymbol{\psi}^D(\boldsymbol{\rho}_{\boldsymbol{\ell}}) = \boldsymbol{\psi}(\boldsymbol{\theta}_{e,\boldsymbol{\ell}}, [0, \rho_{[1,\ell_1]}, \ldots, \rho_{[p-1,\ell_{p-1}]}]),\\ &\boldsymbol{\psi}^D : \mathbb{T}^{p-1} \mapsto \mathbb{R}^{n\times n}, \qquad \rho_{[i,\ell_j]} \in \mathbb{R} \mod 2\pi\\ &\boldsymbol{\ell} = [\ell_1, \ldots, \ell_{p-1}], \qquad \ell_j \in [1, \ldots, N_{\psi,i}]\\ &N_{\mathrm{Ch}} = \textstyle\prod_{i=1}^{p-1} N_{\psi,i} \end{aligned} \tag{75}$$

Here, $\boldsymbol{\ell}$ is an index identifying the corresponding values of $\rho_{[i,\ell_j]}$, $(i, j = 1, \ldots, p-1)$ on an equally space grid over the boundary (cf. Fig. 5). *Second*, the unknown fundamental matrix function values between the N_{Ch} known $\boldsymbol{\psi}^D(\boldsymbol{\rho}_{\boldsymbol{\ell}})$ are interpolated by $(p-1)$ dimensional cubic splines, which gives the continuous approximation function $\boldsymbol{\psi}^{\mathrm{Aprx}}(\boldsymbol{\rho})$. Note that other interpolation methods can equally be used.

Using this interpolated fundamental matrix function $\boldsymbol{\psi}^{\mathrm{Aprx}}(\boldsymbol{\rho})$, any arbitrary set of vectors can be mapped from position $\boldsymbol{\rho}$ on the first boundary to the corresponding position on the opposite boundary.

In particular, the mapping used in Eq. (75) can be evaluated for every possible position on the torus and therefore, the evolution of $V_{m,i}$ may be evaluated arbitrarily long as described above.

In conclusion, the stability assessment of quasi-periodic motions by a combination of the approaches for periodic and general solutions provides an universally applicable method to identify the spectrum of 1st order LYAPUNOV-exponents. The basis is the investigation of perturbations, whose evolution can be described by a fundamental matrix function. Since the perturbations are assumed to be small, they can be described by means of a linearization about the underlying solution torus.

The periodicity of these coordinates enables the construction of a fundamental matrix function by interpolation over a periodic boundary solely based on a few supporting points. Thus, the perturbation evolution description over the *entire quasi-periodic motion*, by which LYAPUNOV-exponents can be identified, is significantly more efficient than with a "brute force" time integration (see also TablerefsecspsAppNonSysspstab3).

4 Application to nonlinear systems

In this section, the proposed method to identify the stability of quasi-periodic motions by means of the spectrum of 1st order LYAPUNOV-exponents is applied to nonlinear dynamical systems to verify and validate it. First of all, a step-by-step instruction is provided in Sect. 4.1 to make the proposed approach more comprehensible by using cross references to the theoretical chapters and to highlight the key steps for an implementation. Subsequently, the approach is applied to two systems exhibiting quasi-periodic motions with two base frequencies ($p = 2$). Although the proposed approach can be used for quasi-periodic motions with a higher base frequency dimension, this contribution focuses on $p = 2$ dimensions and corresponding systems from the literature for the sake of clarity. Restricting to quasi-periodic motions with two base frequencies, three scenarios are possible:

I. two unknown frequencies ω_1 and ω_2,
II. one known Ω and one unknown frequency ω *or*
III. two known frequencies Ω_1 and Ω_2.

In the following, the cases I and III are investigated to demonstrate general applicability, because case II is simply a mixture of the latter two.

In order to *verify* the developed approach, a system of two coupled VAN- DER- POL oscillators (case I) is analyzed in Sect. 4.2. The spectrum of 1st order LYAPUNOV-exponents is computed with the proposed approach as well as with an established method from the literature, the CGSO, which computes the spectrum by means of a brute force time simulation. The two approaches are also compared in terms of numerical cost.

In order to *validate* the approach, a quasi-periodically forced DUFFING equation (case III) is investigated. A reference is made between the identified results and findings from the literature as well as a direct comparison with time simulations.

All computed results are identified with the simulation program QUONT, which has been implemented in MATLAB and has been developed in the dissertation thesis of the first author [18].

4.1 Step-by-step instructions for application

In this subsection, the required steps for an implementation of the stability identification method in a numerical tool are discussed. By applying the following instruction, the spectrum of 1st order LYAPUNOV-exponents can be identified, with which the stability of quasi-periodic motions can be characterized.

Required steps

Step 1.) *Calculate* the torus function $\boldsymbol{Z}(\boldsymbol{\theta})$ of the quasi-periodic motion of interest by solving the partial differential Eq. (10) with either a finite difference method, a FOURIER- GALERKIN method or a comparable method. Alternatively, solve the ordinary differential Eq. (12) by means of a shooting method for quasi-periodic motions to obtain a finite set of characteristics of the torus function $\boldsymbol{Z}(\boldsymbol{\theta}(t))$.

Step 2.) *Calculate or identify* all values of the JACOBIAN-matrix function $\boldsymbol{J}(\boldsymbol{\theta})$ on the coordinate torus $\boldsymbol{\theta}$ in order to solve Eq. (62) from boundary-to-boundary by means of a time integration. If the shooting method for quasi-periodic motions is applied, one can jump directly to step 5.) because discrete fundamental solutions $\boldsymbol{\psi}^D$ along the characteristics are known due to the involved solution process of the nonlinear equation system (e.g., NEWTON-method).

Step 3.) *Choose* discretization points on the periodic boundary (cf. Fig. 5) and evaluate the continuous matrix functions $\boldsymbol{\psi}(\boldsymbol{\theta}_e, \boldsymbol{\theta}_s)$ to obtain discrete matrices $\boldsymbol{\psi}^D$. The choice of the periodic boundary can be arbitrarily, because each boundary is suitable for this method. One should only be aware that the integration time (cf. Eq. (67a)) depends on the chosen boundary. The authors suggest taking the largest frequency ν_{max}.

Step 4.) *Solve* Eq. (62) at the chosen discrete supporting points over the time interval $\tau \in [0, \frac{2\pi}{\nu_{max}}]$ to obtain discrete fundamental matrices (cf. Eq. (75)), which map perturbations boundary-to-boundary. Choose as initial value the identity matrix to identify normalized fundamental matrices.

Step 5.) *Interpolate* the values between the supporting point fundamental matrices, which where chosen or given by applying a *shooting method*, by means of e.g., $p-1$ dimensional cubic splines (cf. Fig. 5) to obtain an approximation to a continuous fundamental matrix function (cf. Eq. (69)). Consequently, perturbations can be mapped arbitrarily form boundary-to-boundary.

Step 6.) *Choose* an arbitrary set of m orthonormal vectors $[\mathbf{e}_1(\tau), \ldots, \mathbf{e}_m(\tau)]$. The first m vectors (cf. Eq. (36)) span the required volumes $V_m(t)$. *Map* the set of m vectors from boundary-to-boundary (cf. Eq. (74)) starting at an arbitrary position on the periodic boundary (e.g., $t = 0$). *Determine* the volumes $V_{m,1}$ of the distorted set of m vectors (cf. Eq. (72)).

Step 7.) *Re-orthonormalize* and therefore *re-normalize* the distorted set of m vectors after each mapping by means of a GRAM- SCHMIDT method. As a result, the volumes are equivalent to one. Repeat the mapping, volume identification and re-orthonormalization process as long as necessary (cf. next step). It is crucial to note that only the initial set of vectors can be chosen arbitrarily. Once mapped, the set *should only* be orthonormalized, by which the dynamical behavior along a trajectory is considered. The re-orthonormalization compensates for the exponential growth or decay of the perturbation in the linear system.

Step 8.) *Calculate* the mth order LYAPUNOV-exponents (cf. Eq. (72)) by means of the identified results, from which the spectrum of 1st order LYAPUNOV-exponents can be derived (cf. Eq. (46)). Because Eq. (72) describes a converging quantity, one can evaluate the influence of each additional map on the accuracy of the exponents and decide how many mappings k are required to obtain the investigation specific precision.

Step 9.) optional: *Check* LYAPUNOV-*regularity* of the linearization as outlined in the last section of 2.2.2. This involves checking the convergence of the mth order exponents—this step can be done simultaneously to the actual calculation of $\sigma^{(n)}$. After repeating these calculations for the adjoint system, Eq. (43) can be checked by comparing both spectra.

4.2 Verification example: two coupled VAN- DER- POL oscillators

In order to *verify* the detailed approach, the spectrum of 1st order LYAPUNOV-exponents is identified by means of the proposed method and by means of an established approach for comparison, the continuous GRAM- SCHMIDT orthonormalization (CGSO) (cf. [13]).

The analyzed dynamical system consists of two linearly coupled VAN- DER- POL oscillators

$$\begin{aligned} \ddot{x} + \varepsilon(x^2 - 1)\dot{x} + x &= \alpha(y - x) \\ \ddot{y} + \varepsilon(y^2 - 1)\dot{y} + (1 + \beta)y &= \alpha(x - y), \end{aligned} \tag{76}$$

where ε is the non-linearity parameter, β is called the detuning parameter and α is the coupling strength. Two arbitrary parameter sets are chosen, which exhibit quasi-periodic motions (see TablerefsecspsAppNon-Sysspstab0).

This system is a classical test example for quasi-periodic oscillations in an autonomous system. It has

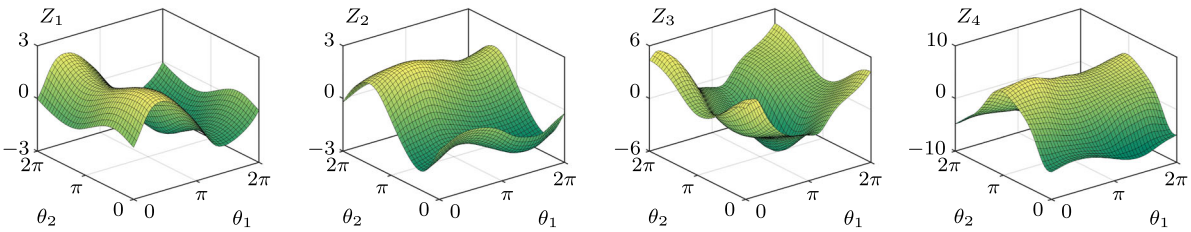

Fig. 6 Torus function of the quasi-periodic motion for set 1 parameterized in hyper time ($\theta_1 = \omega_1 t$ and $\theta_2 = \omega_2 t$)

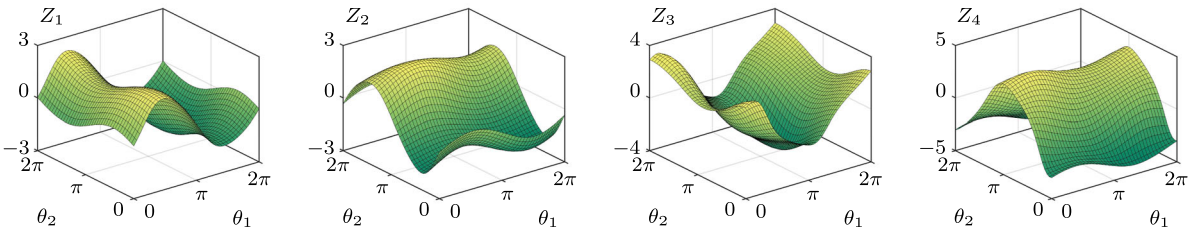

Fig. 7 Torus function of the quasi-periodic motion for set 2 parameterized in hyper time ($\theta_1 = \omega_1 t$ and $\theta_2 = \omega_2 t$)

Table 1 Parameter sets for verification example in Eq. (76)

	Set 1 cf. [42, Fig. 4]	Set 2 cf. [43, Fig. 13]
ε	0.5	1
α	0.5	2
β	1.5	5

Table 2 Parameters and computed 00results of both torus functions approximated by a finite difference method

	Set 1	Set 2
Discretization mesh	61×61	61×61
characteristics (N_{Ch}, Eq. (75))	61	61
ω_1	1.1612	1.4953
ω_2	1.7483	2.8917
e_{rr}	$4.4384 \cdot 10^{-4}$	$6.0066 \cdot 10^{-4}$

extensively been investigated and is known to exhibit regular behavior in the sense of LYAPUNOV. Thus, regularity may be assumed.

In a first step, Eq. (76) is written as a first order ODE

$$[\mathrm{z}_1, \mathrm{z}_2, \mathrm{z}_3, \mathrm{z}_4] = [x, y, \dot{x}, \dot{y}] \tag{77}$$

and transformed into an invariance equation. Subsequently, the torus function $\boldsymbol{Z} = [Z_1, Z_2, Z_3, Z_4]$ is identified by solving Eq. (10) and Eq. (11) with a finite difference method, by which the quasi-periodic motions are identified.

The results of the local point approximation of the finite difference method are depicted in Figs. 6 and 7. In Table 2 some relevant parameters and results of both computations are summarized.

Both manifolds are approximated using an equidistant mesh with 61 nodes in θ_1- and 61 nodes in θ_2-direction. Furthermore, sixth order central difference schemes are used to approximate the differentials in Eq. (10).

In order to estimate the approximation error e_{rr} of the computed results, an embedded method is used. Therefore, the torus function is calculated again, but instead of using a sixth order central difference scheme, a fourth order difference scheme is used. The error is estimated by identifying the relative difference

$$\mathrm{e}_{rr} = \left| \frac{\tilde{\boldsymbol{Z}}_{6\mathrm{th}} - \tilde{\boldsymbol{Z}}_{4\mathrm{th}}}{\tilde{\boldsymbol{Z}}_{6\mathrm{th}}} \right|, \tag{78}$$

where $\tilde{\boldsymbol{Z}}_{6\mathrm{th}}$ and $\tilde{\boldsymbol{Z}}_{4\mathrm{th}}$ are the solution vectors of the sixth and forth order approximation, respectively.

Considering Figs. 6 and 7, both torus functions appear qualitatively similar. Regarding the identified free frequencies ω_1 and ω_2 (cf. Table 2), it is obvious that each torus function is filled differently by the

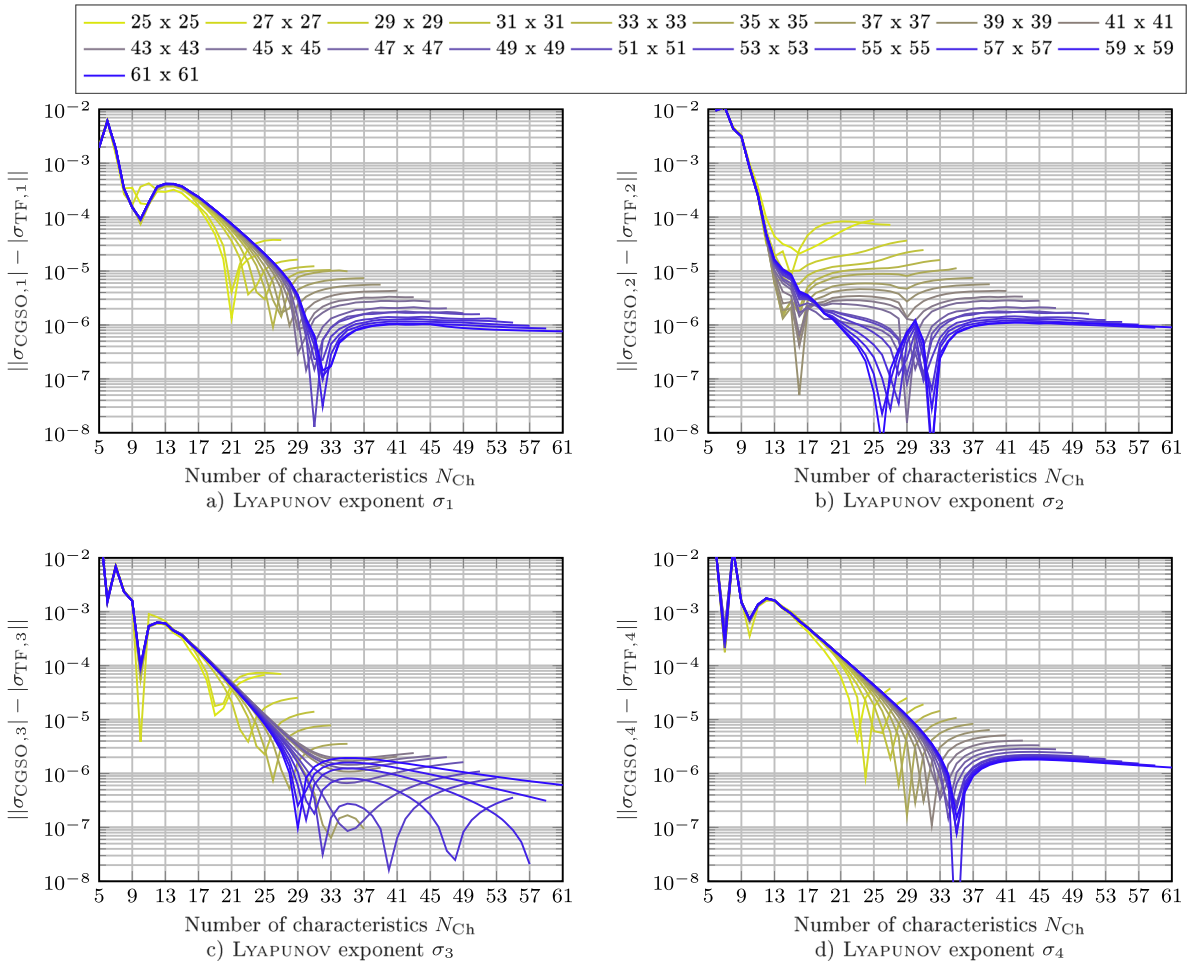

Fig. 8 LYAPUNOV-exponents of parameter set 1 identified with the CGSO in comparison with different equidistant discretization grids (indicated by the line color) and a varying number of characteristics N_{Ch} of the presented approach based on the torus function. (Color figure online)

underlying quasi-periodic motion ($\theta_1 = \omega_1 t, \theta_2 = \omega_2 t$).

In order to get a reference solution for the spectra of 1st order LYAPUNOV-exponents, the CGSO is utilized to identify a reference solution. Because the CGSO is based on a time integration, the `ode45` function[20] (explicit RUNGE-KUTTA-scheme with DORMAND-PRINCE (4,5) pair [17]) in MATLAB is used to solve the equation system. To keep the transient behavior minimal, initial values are chosen, which are located on the quasi-periodic invariant tori.

All results presented in Table3 are computed on the basis of a very large time interval $t = [0, T_p] = [0, 10^7]$. The number of iterative mappings $N_{map} = \frac{T_p}{\frac{2\pi}{\omega_2}} = \frac{10^7}{\frac{2\pi}{\omega_2}}$ used for the presented approach corresponds the physical time interval T_p of the *CGSO*.

It can be seen that this considerable large time interval is necessary to obtain a magnitude of accuracy of the *CGSO* of approximately 10^{-8}. This can be identified by investigating σ_1 and σ_2, which both have to be equal to zero, because they describe the separation rate in tangential direction of the torus. As can be seen from the numerical values of the LYAPUNOV-exponents given in Table3, the solutions are stable for both param-

[20] In comparison with other available MATLAB integrators, the `ode45` had the lowest computational cost for a set accuracy. The algorithm controls the error by using an embedded error estimator and step width control.

Table 3 Comparison of the spectra of 1st order LYAPUNOV-exponents σ. Number of mapping N_{map} is equal to physical time T_p

	Set	CGSO	Torus function 61×61	Difference (absolute)
	1	$T_p = 1 \cdot 10^7$ s	$N_{\text{map}} \approx 2.7 \cdot 10^6$	
	2	$T_p = 1 \cdot 10^7$ s	$N_{\text{map}} \approx 4.6 \cdot 10^6$	
1	σ_1	$-4.5275 \cdot 10^{-8}$	$-8.0624 \cdot 10^{-7}$	$7.61 \cdot 10^{-7}$
	σ_2	$4.5826 \cdot 10^{-8}$	$-9.4979 \cdot 10^{-7}$	$9.96 \cdot 10^{-7}$
	σ_3	-0.27619516	-0.27619455	$6.11 \cdot 10^{-7}$
	σ_4	-0.52350145	-0.52350016	$1.29 \cdot 10^{-6}$
2	σ_1	$6.7325 \cdot 10^{-8}$	$-2.616587 \cdot 10^{-6}$	$2.68 \cdot 10^{-6}$
	σ_2	$6.5722 \cdot 10^{-8}$	$-4.070997 \cdot 10^{-6}$	$4.14 \cdot 10^{-6}$
	σ_3	-0.38552093	-0.38552099	$6.88 \cdot 10^{-6}$
	σ_4	-1.07304917	-1.07304880	$1.67 \cdot 10^{-5}$

eter sets: two exponents are zero (within the numerical accuracy) and the two remaining ones are negative.

Considering the results obtained with the described method by using the torus functions, the results are in very good agreement with the *CGSO*. Concerning set 1, the accuracy of the proposed method is equivalent to the CGSO. Concerning set 2, the accuracy deviates slightly, although the accuracy is still very high. This deviation stems from the higher degree of nonlinearity ($\varepsilon = 1$), which results in slightly more complicated torus functions. This would require a finer mesh for an equivalent approximation error compared to set 1 (cf. e_{rr}, Table2).

In order to investigate the influence of the numerical parameter N_{Ch} (i.e., the number of characteristics used for interpolation) on the spectrum of 1st order LYAPUNOV-exponents, the results for different N_{Ch} and different torus FD discretizations are compared to results of the CGSO. Arbitrarily, set 1 is chosen to perform this analysis. The investigation is conducted by starting with five characteristics ($N_{\text{Ch}} = 5$) and this number is increased until the number of nodes on the periodic boundary is reached (FD-discretization: 61). A number of characteristics larger than the number of FD-nodes on a boundary would not be reasonable, because the accuracy of the fundamental matrix function interpolation would not increase.

The results are presented in Fig. 8, where in each figure the difference of the identified LYAPUNOV-exponents is plotted over the number of characteristics N_{Ch}. Considering the results for low N_{Ch} in Fig. 8, each FD discretization provides almost equal exponents. Because the approximation of the fundamental matrix function is rough when considering a low number of characteristics, the underlying approximation of the torus function does not play a significant role.

It seems that each LYAPUNOV-exponent exhibits for each discretization some sort of minimum. Analyzing the minima, their occurrence for each exponent is located at different numbers of characteristics, by which these minima are the result of a coincidental well approximated exponent.

In addition, one has to keep in mind that the CGSO only ensures an approximation accuracy of approximately 10^{-8}, by which the identified results in this magnitude should be interpreted with caution. For a larger number of characteristics, the errors saturate or drop only slightly when the discretization is kept fixed. This may imply that the error introduced by the cubic spline interpolation is reduced as far as almost possible. Stated differently, further increasing the number of supporting points (characteristics) for the interpolation does not lead to a significantly higher approximation quality of the fundamental matrix function based on the current discretization. At that stage, the error is controlled almost entirely by the discretization of the torus itself. Consequently, accuracy can be controlled by a combination of FD discretization and a number of characteristics, whereas uniform convergence occurs when the number of characteristics is chosen to be similar to the FD discretization. As a last point, a comparison of computational cost[21] between the *CGSO* and the *presented method* is carried out. The results are listed in Table4. The comparison is done for the two parameter sets 1 and 2 in Table1. Here, the computation is carried out until the value of the first LYAPUNOV exponent—which should theoretically be zero—converged[22] to

[21] All simulations for the computational cost comparison were done with MATLAB R2021a on a workstation with an Intel® Xeon® CPU E5-2643 @ 3.30 GHz, 4 cores and 128 GB of RAM. For the simulations with the presented methods, the time mean value for 100 simulations is noted. The noted computation cost for the *CGSO* for set 2 A) is the mean value of 20 identical simulations.

[22] Since LYAPUNOV-exponents tend to oscillate with time around a mean value (and therefore also number of mappings) (see e.g., [20]), the floating mean value for the last 100 physical seconds was used. For larger floating time windows, the convergence time changed only insignificantly. In order to assure comparable conditions for the computation, the initial values for the *CGSO* were chosen on the torus function $\boldsymbol{Z}(0, 0)$ used as basis by the proposed method.

$A) : \sigma_1 \approx 10^{-4}$ and $B) : \sigma_1 \approx 10^{-5}$. For both the *CGSO* and the proposed method, the necessary simulated time T_p and the (physical) computational time T_c are noted. In case of the presented method, T_c is the sum of the time T_ψ needed to construct the fundamental matrix function and the time T_{Ma} for the execution of the N_{map} mappings.

In the last column of Table 4 the relative reduction of computational cost by using the presented method over the CGSO is noted. The reduction for T_{Ma} is given w.r.t. T_c of the *CGSO*.

Here, a few observations are noteworthy: The reduction in computational cost w.r.t. the *CGSO* is significant. For the four examples, the cost is reduced by at least 94% between the *presented method* and the *CGSO*. The greater part of the computational effort T_ψ is spent on the construction of the basic matrix function $\boldsymbol{\psi}^D$. This construction is not necessary, if the described quasi-periodic shooting method is used in which case a reduction of over 99% is achieved. It is also interesting that the physical time T_p, which has to be simulated with both methods, is in the same order of magnitude. Please also note the reduction in convergence speed of both methods for increasing the accuracy from $A) : \sigma_1 \approx 10^{-4}$ to $B) : \sigma_1 \approx 10^{-5}$.

Concluding, the proposed method provides very accurate results, whilst being rather efficient. The basis of the stability approximation approach is a linearization around a computed solution. Consequently, the identification of stability measurement, here the spectrum of 1st order LYAPUNOV-exponents, depends on the underlying approximation accuracy. Because this approach enables an approximation of the fundamental matrix function on one periodic boundary, the accuracy can be controlled. The latter enables a highly time efficient approach, if a lower accuracy is acceptable.

It is also important to stress again that this method *does not* depend on the chosen discretization approach and can be used generally for continuous torus functions.

4.3 Validation example: quasi-periodically forced DUFFING equation

Having *verified* the developed approach, the proposed method is *validated* by applying it to a bi-periodically forced DUFFING equation

$$\ddot{x} + 2\zeta\dot{x} + x + \xi x^3 = f_1 \sin(\Omega_1 t) + f_2 \sin(\Omega_2 t). \tag{79}$$

Table 4 Comparison of computational cost for parameter set 1 and 2 (Table 1) and for reaching A: $|\sigma_1| \approx 10^{-4}$, B: $|\sigma_1| \approx 10^{-5}$. T_p : physical time; T_c : computation time; T_ψ : time for computing fundamental matrix function; T_{Ma} : time for mapping; N_{Ma} : Number of mappings

Set	CGSO	Torus function (61×61)	Relative reduction (w.r.t. CGSO)
1: A)			
T_p	3500 s	3917 s	−0.1192
T_c	52.307 s	2.836 s	0.9406
T_ψ	–	2.758 s	–
T_{Ma}	–	0.078 s	0.9984
N_{map}	–	1090	–
1: B)			
T_p	37250 s	35, 938 s	0.0352
T_c	551.643 s	3.233 s	0.9931
T_ψ	–	2.624 s	–
T_{Ma}	–	0.610 s	0.9986
N_{map}	–	10000	–
2: A)			
T_p	6575 s	6790 s	−0.0327
T_c	96.741 s	3.216 s	0.9625
T_ψ	–	3.030 s	–
T_{Ma}	–	0.186 s	0.9976
N_{map}	–	3125	–
2: B)			
T_p	65, 000 s	48, 898 s	0.2480
T_c	965.461 s	4.7239 s	0.9948
T_ψ	–	3.211 s	–
T_{Ma}	–	1.5132 s	0.9983
N_{map}	–	22,500	–

Equation (79) exhibits the advantage that incommensurable values can be chosen for the two known frequencies Ω_1 and Ω_2. Thus, the resulting motion is expected to be quasi-periodic. Another aspect, classifying Eq. (79) as a well suited validation example, is the fact that two sources from the literature [23,33] have analyzed the stability of the resulting quasi-periodic motion by different approaches (cf. Sect. 1). Both used methods to approximate the torus function based on the multi-dimensional harmonic balance, which is almost identical to the FOURIER- - GALERKIN method. In this contribution, a finite difference method is used to identify the torus functions (cf. [18]).

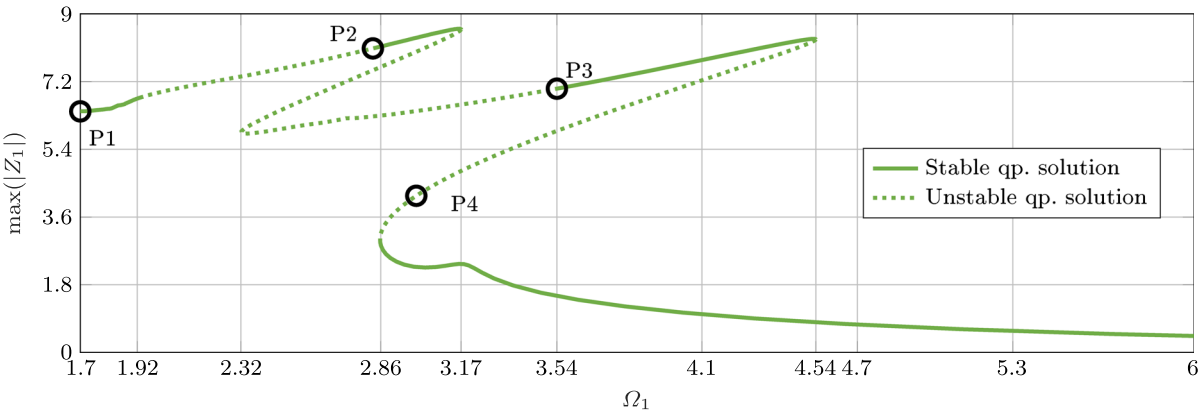

Fig. 9 Computational results of the continuation with an included stability analysis for the quasi-periodically forced DUFFING equation

The parameters are chosen equivalently to the references [23] and [33]:

$$\zeta = 0.1, \quad \xi = 0.2, \quad f_1 = f_2 = 5, \quad \Omega_2 = \frac{\Omega_1}{\sqrt{2}}. \tag{80}$$

The parameter Ω_1 is varied in the interval [1.7, 6].

In order to get a comprehensive picture of the results, a continuation algorithm is used (cf. [46, chapter 4]). Specifically, the continuation variable is Ω_1, the process is initiated at $\Omega_1 = 6$ and a pseudo arc-length method is used to continue the results.

The discretization of the torus functions is kept constant with 61 x 61 nodes. Since the topologies of torus functions along the solution paths are partly complicated, the number of characteristic supporting points is kept at its practical relevant maximum value $M = 61$.

Transforming Eq. (79) into state-space $[z_1, z_2] = [x, \dot{x}]$ and identifying the torus functions $\boldsymbol{Z} = [Z_1, Z_2]$ by solving Eq. (10) with a finite difference method (sixth order central differences), the quasi-periodic motions are identified (s. Fig. 9).

Comparing Figs. 6 to 9 in [23] and Fig. 10 in [33], the results are *qualitatively* equivalent. Figure 9 depicts the two characteristic peaks, which, roughly speaking, stem from the DUFFING's equation typical nonlinear resonances of each individual excitation $f_1 \sin(\Omega_1 t)$ and $f_2 \sin(\Omega_2 t)$. Please note, that in the figures of [23] and [33] the norm of the FOURIER coefficients is plotted on the ordinate and not the maximum deflection of x.

In order to get a deeper understanding of the identified results, Figs. 10, 11 and 12 depict the identified spectrum of 1st order LYAPUNOV-exponents, their convergence and the estimated error of the torus function (cf. Eq. (78)). All figures depict the results *along the continuation* path, which corresponds to the arc-length of the solution curve illustrated in Fig. 9. For the purpose of orientation, the stability changes are marked by the corresponding Ω_1-value in Figs. 10, 11 and 12. Considering the spectrum of 1st order LYAPUNOV-exponents in Fig. 10, only two values are computed, because the tangential space and, thus, the two exponents equal to zero stem from the forcing mechanisms. This is equivalent to a monodromy matrix of a periodic motion stemming from a forced system, which does not exhibit the FLOQUET-multiplier equal to 1. Regarding Fig. 10, a clear and plausible progression of the exponents is identified.

The largest LYAPUNOV-exponent σ_1 always changes its sign, once a stability change is encountered. At each stability change, there exists a point where $\sigma_1 = 0$. This indicates a non-hyperbolic solution, where bifurcations of the quasi-periodic motion occur, because the contraction or divergence behavior of the normal space is "indifferent". As far as the authors are aware, a directly applicable bifurcation theory based on the LYAPUNOV-exponents does not exists, by which the classification of the identified bifurcations is impossible. Nevertheless, considering $\Omega_1 \in [3.17, 2.32, 4.54, 2.86]$ and comparing it to Fig. 9, suggests that the identified bifurcation can be classified as a *limit point 2-torus* bifurcation. The latter nomenclature is a generalization of a *limit point* bifurcation (fold-bifurcation of an equilibrium) and a *limit point cycle* bifurcation (fold-bifurcation of a periodic motion).

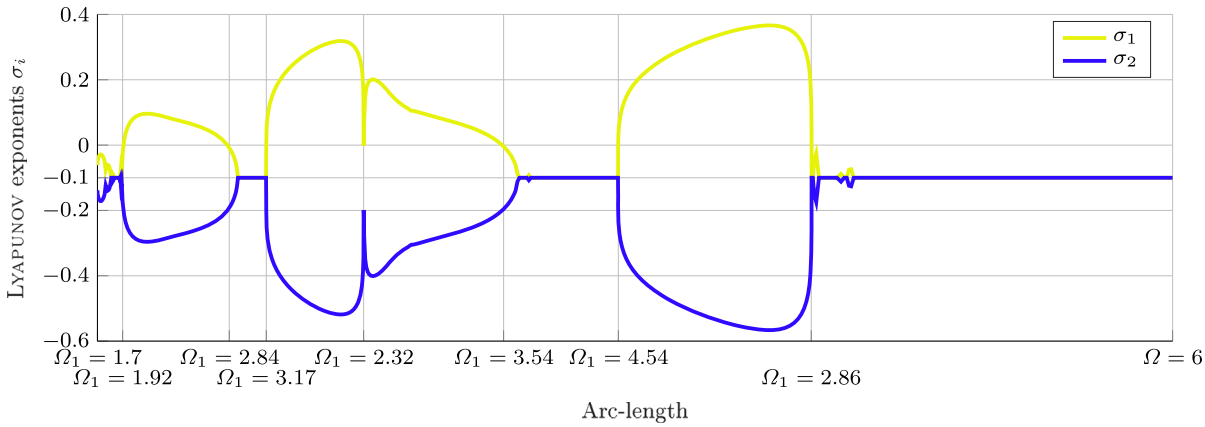

Fig. 10 Computed spectrum of 1st order LYAPUNOV-exponents plotted over the arc-length of the continuation for the quasi-periodically forced DUFFING equation

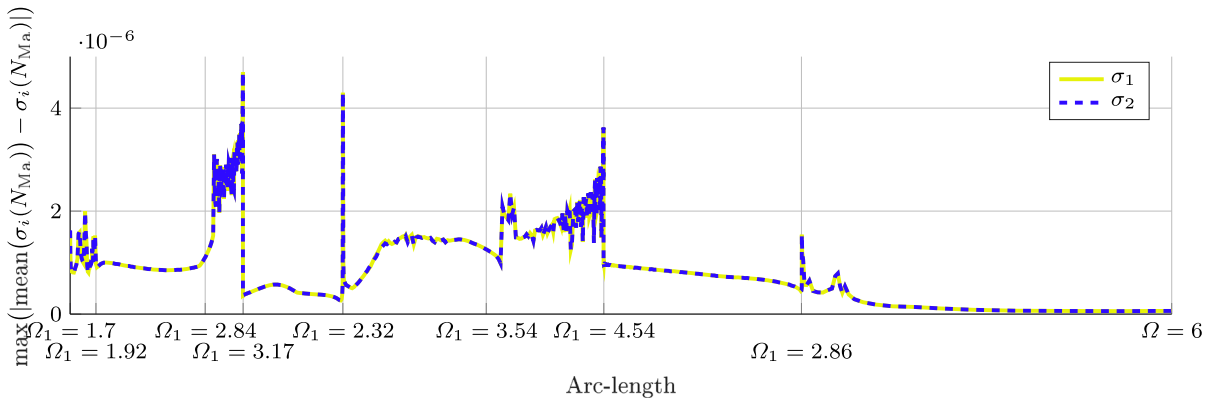

Fig. 11 Maximal absolute deviation between the mean value of the LYAPUNOV exponent mean(σ_i) and the value of σ_i both w.r.t. the last 100 physical seconds of mapping. Graphs plotted over the arc-length of the continuation for the quasi-periodically forced DUFFING equation

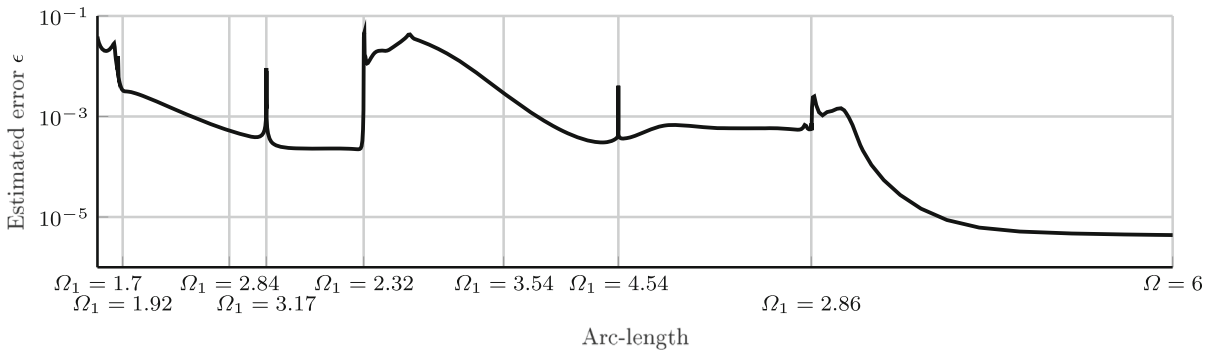

Fig. 12 Computed error estimation according to Eq. (78) plotted over the arc-length of the continuation for the quasi-periodically forced DUFFING equation

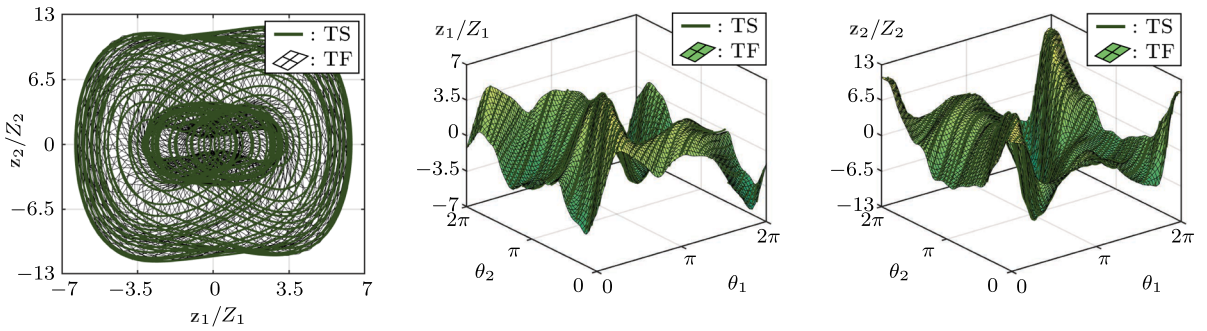

Fig. 13 Stable motion at $\Omega_1 = 1.7$ ($[\sigma_1, \sigma_2, \sigma_3, \sigma_4] = [0, 0, -0.0616, -0.1384]$): Computational results of the torus function (TF) $\boldsymbol{Z}(\theta_1, \theta_2) : \mathbb{T}^2 \mapsto \mathbb{R}^2$ on a 61×61 mesh and the time simulation (TS) at P1 (cf. Fig. 9). Trajectory predicted by TS stays on the torus indicating stable behavior

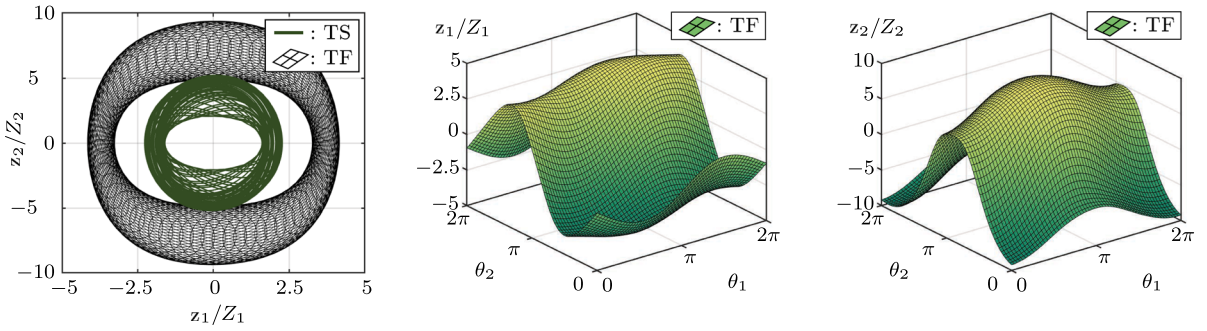

Fig. 14 Unstable motion at $\Omega_1 = 2.997$ ($[\sigma_1, \sigma_2, \sigma_3, \sigma_4] = [0.3407, 0, 0, -0.5407]$): Computational results of the torus function (TF) $\boldsymbol{Z}(\theta_1, \theta_2) : \mathbb{T}^2 \mapsto \mathbb{R}^2$ on a 61×61 mesh and the time simulation (TS) at P4 (cf. Fig. 9). Trajectory predicted by TS diverges from the torus indicating unstable behavior

An additional aspect verifying the identified spectrum of 1st order LYAPUNOV-exponents, is the constant 2nd order LYAPUNOV-exponent $\sigma^{(2)} = \sigma_1 + \sigma_2$. Regarding Fig. 10, $\sigma^{(2)} = -0.2 \quad \forall \Omega_1$ holds, which can easily be verified analytically [1, Eq. (5.4.83)], as

$$\begin{aligned} \sigma^{(2)} &= \lim_{T\to\infty} \frac{1}{T} \int_0^T \operatorname{div} \mathbf{f}(\mathbf{z}(t)) \mathrm{d}t \\ &= \lim_{T\to\infty} \frac{1}{T} \int_0^T -2\zeta \, \mathrm{d}t = -0.2, \end{aligned} \tag{81}$$

where $\mathbf{z}(t)$ is the state space vector and $\mathbf{f}(\mathbf{z}(t))$ is the vector field of Eq. (79). The divergence in Eq. (81) is a measure of sources or sinks in a vector field and is, therefore, related to the changes over time of a specific volume that is exposed to that vector field. The LYAPUNOV-exponent of order m is equivalent to the time average of the divergence and always negative for dissipative systems.

Figure 11 shows the deviation of the LYAPUNOV-exponents $\sigma_{1,2}$ for the last equivalent 100 physical seconds of the mapping procedure from the mean value of that time mean$(\sigma_{1,2}(N_{\text{map}}))$. This shows that both exponents are sufficiently convergent with a deviation smaller than $1 \cdot 10^{-5}$.

Regarding Fig. 12, it is interesting to note that the approximation error increases in the vicinity of the limit point 2-torus bifurcations, because similar behavior is not observable for the remaining stability changes at $\Omega_1 \in [1.92, 2.84, 3.54]$. Another noteworthy observation is the reduced accuracy for small Ω_1, which stems from an increased complexity of the torus function.

Having validated the computational results *qualitatively*, only the *quantitative* verification is left open.

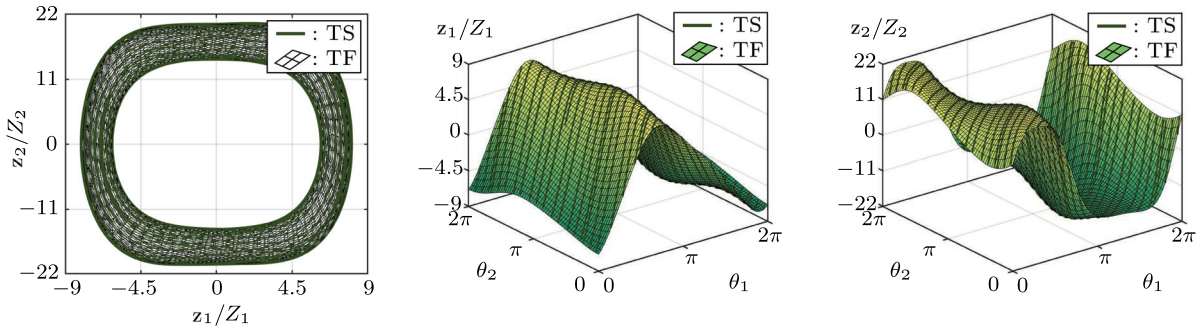

Fig. 15 Stable motion at $\Omega_1 = 2.839$ ($[\sigma_1, \sigma_2, \sigma_3, \sigma_4] = [0, 0, -0.0038, -0.1962]$): Computational results of the torus function (TF) $\boldsymbol{Z}(\theta_1, \theta_2) : \mathbb{T}^2 \mapsto \mathbb{R}^2$ on a 61 x 61 mesh and the time simulation (TS) at the *stable side* of P2 (cf. Fig. 9). Trajectory predicted by TS stays on the torus indicating stable behavior

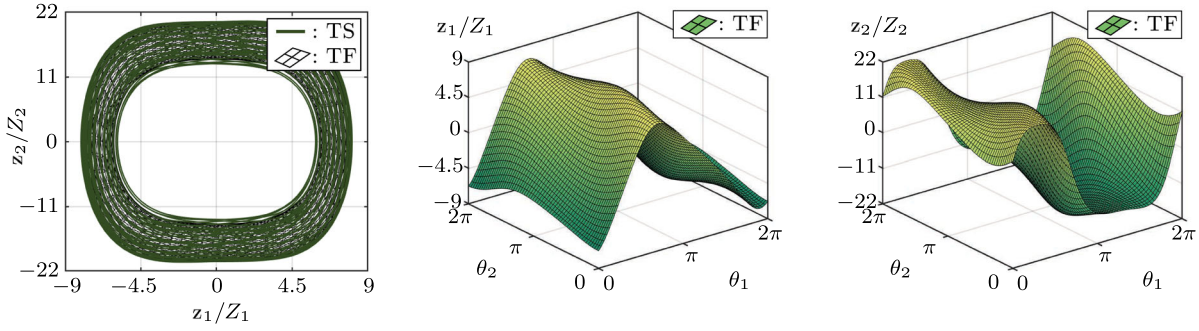

Fig. 16 Unstable motion at $\Omega_1 = 2.820$ ($[\sigma_1, \sigma_2, \sigma_3, \sigma_4] = [0.0046, 0, 0, -0.2046]$): Computational results of the torus function (TF) $\boldsymbol{Z}(\theta_1, \theta_2) : \mathbb{T}^2 \mapsto \mathbb{R}^2$ on a 61 x 61 mesh and the time simulation (TS) at the *unstable side* of P2 (cf. Fig. 9). Trajectory predicted by TS diverges from the torus indicating unstable behavior

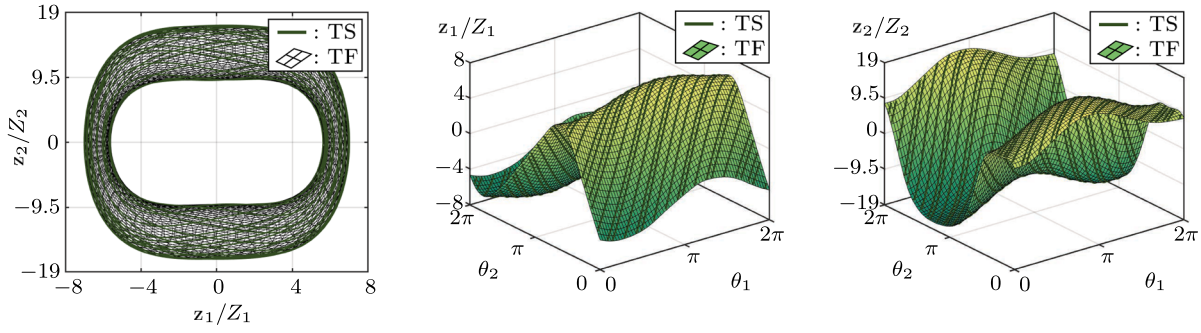

Fig. 17 Stable motion at $\Omega_1 = 3.54$ ($[\sigma_1, \sigma_2, \sigma_3, \sigma_4] = [0, 0, -0.0040, -0.1960]$): Computational results of the torus function (TF) $\boldsymbol{Z}(\theta_1, \theta_2) : \mathbb{T}^2 \mapsto \mathbb{R}^2$ on a 61 x 61 mesh and the time simulation (TS) at the *stable side* of P3 (cf. Fig. 9). Trajectory predicted by TS stays on the torus indicating stable behavior

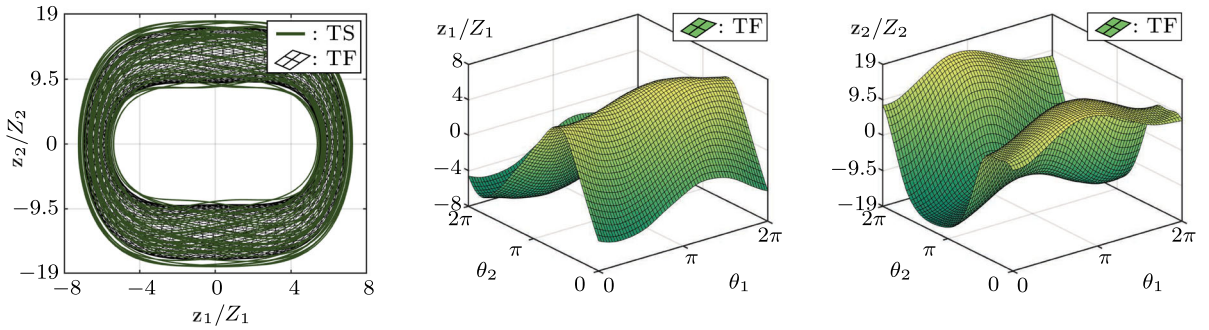

Fig. 18 Unstable motion at $\Omega_1 = 3.522$ ($[\sigma_1, \sigma_2, \sigma_3, \sigma_4] = [0.0018, 0, 0, -0.2018]$): Computational results of the torus function (TF) $\boldsymbol{Z}(\theta_1, \theta_2) : \mathbb{T}^2 \mapsto \mathbb{R}^2$ on a 61 x 61 mesh and the time simulation (TS) at the *unstable side* of P3 (cf. Fig. 9). Trajectory predicted by TS diverges from the torus indicating unstable behavior

This comparison is conducted by means of a time integration of Eq. (79) in state-space form for which the `ode45` function (explicit RUNGE- KUTTA-scheme using a DORMAND- PRINCE (4,5) pair [17]) in MATLAB is used. The time simulation is initiated on the torus function and the time interval is chosen such that a stationary motion is identified.

Subsequently, the result depictions in Fig. 13, 14, 15, 16, 17 and 18 are organized as follows:

- *Left hand side:* A torus function projection and a section of the resulting stationary quasi-periodic motion are depicted in state-space.
- *Middle:* The torus function $Z_1(\theta_1, \theta_2)$ and, if stable, a section of the resulting stationary quasi-periodic motion of $z_1(t)$ obtained by time simulations are depicted in torus domain $[\theta_1, \theta_2] \in \mathbb{T}^2$.
- *Right hand side:* The torus function $Z_2(\theta_1, \theta_2)$ and, if stable, a section of the resulting stationary quasi-periodic motion of $z_2(t)$ obtained by time simulations are depicted in torus domain $[\theta_1, \theta_2] \in \mathbb{T}^2$.

Arbitrarily, the two points P1 and P4 (cf. Fig. 9) are exemplary chosen to verify the results in general. The results are depicted in Figs. 13 and 14. As predicted by the algorithm, the time simulation verifies that the quasi-periodic motion is stable at P1 and unstable at P4: the trajectory initialized on the torus stays on the torus or diverges from it. Although the estimated error of the results at P1 are relatively high (cf. Fig. 12), the predicted torus function captures the underlying quasi-periodic motion very well.

In order to demonstrate the accuracy of the proposed method, two arbitrarily chosen predicted stability changes are investigated. Regarding the identified limit point 2-torus bifurcations, the transition from a stable to an unstable quasi-periodic motion is plausible. Consequently, two of the additionally appearing stability transitions are investigated (P2 and P3). The results are verified by investigating in a similar manner as described above the stable and unstable side of the transition (s. Fig. 15, 16, 17 and 18).

Considering Figs. 15 and 16 and Figs. 17 and 18, an equivalent behavior can be observed. First, the stability of the quasi-periodic motion is predicted correctly. Second, because the continuation parameter change is marginally, in both cases the torus functions are almost identical. Nevertheless, the stability characteristic of the quasi-periodic motion changes within the regarded intervals, which is verified by time simulation: in both unstable cases, another quasi-periodic torus solution is approached by the trajectory. These motion may stem from a quasi-periodic period doubling bifurcation occurring at these stability changes (cf. [23]). Because this contribution focuses on the stability identification method, the latter findings are not further pursued in this work.

Concluding this subsection, the usefulness of the presented approach has been validated qualitatively and quantitatively by means of a quasi-periodically forced DUFFING equation. The computational results have been validated qualitatively by comparing the continuation path with findings from the literature. Furthermore, a quantitative validation of the identified stability characteristics has been conducted by initiating time simulations on exemplary torus functions. Besides the time simulations, the analytical criterion of Eq. (81)

validates the identified LYAPUNOV-exponents (cf. Figs. 13, 14, 15, 16, 17 and 18).

5 Conclusion

In this contribution, an approach to efficiently calculate the LYAPUNOV- exponents of quasi-periodic solutions is presented. For regular systems, these results may be used to assess the stability of the considered solutions.

The basic idea is similar to the standard approach for periodic problems, where the mapping over one period—the monodromy-matrix—is used to assess stability. Different to periodic problems, for quasi-periodic systems the notion of periodicity is not obvious beforehand and it is not possible to identify a single characteristic mapping similar to the monodromy matrix. Within this contribution, the periodicities inherent to quasi-periodic problems are identified and a matrix function is introduced which allows efficient iterations of mappings over arbitrarily long time intervals. Based on this, an efficient calculation of LYAPUNOV-exponents is possible.

To this end a hyper-time parametrization of the investigated quasi-periodic motion is introduced, which allows to describe the invariant manifold by means of torus functions: eventually, these torus functions reveal generalized periodicities inherent to the problem. These periodicities allow for a systematical formulation of an arbitrarily long sequence of mappings by means of a simple interpolation of a priori calculated fundamental matrices. Based on this sequence of mappings the spectrum of 1st order LYAPUNOV-exponents may then efficiently be calculated with arbitrary precision by means of a standard re-orthonormalization technique. For systems whose linearizations are LYAPUNOV regular, their stability can be derived from the calculated LYAPUNOV-exponents. Please note that this approach is actually independent of the method chosen to determine the torus manifold on which the quasi-periodic motion is embedded. Consequently, it may for instance be applied to FOURIER-GALERKIN approaches as well as to shooting approaches.

The presented method has been verified and validated by application to two nonlinear dynamical systems and the results were analyzed. First, as verification example, a system of two coupled VAN- DER- POL oscillators has been analyzed by means of the proposed method as well as by using an established method, namely the continuous GRAM- SCHMIDT orthonormalization. The accuracy of the identified LYAPUNOV-exponents dependents on the resolution of the computed underlying torus solution, the number of characteristics and the number of mappings. A sufficient convergence of the values of the exponents must thus be checked and assured. The presented method significantly outperforms the GRAM- SCHMIDT orthonormalization for this example in terms of computational cost and also can be applied to unstable quasi-periodic motions, which are the main advantages. As validation example, a quasi-periodically forced DUFFING equation has been investigated. The computational results of the proposed method coincide with results available in the literature and a comparison with time simulations initiated on the identified torus functions (quasi-periodic invariant manifolds) confirm the predicted stability characteristics. Furthermore the investigation revealed other branches of quasi-periodic solutions, which have been identified at the investigated stability changes (bifurcation points) and will be analyzed in future works.

Author contributions All authors contributed to the presented research. Overall material preparation, data collection, numerical implementation as well as corresponding numerical analysis were performed by Robert Fiedler. The presented method for stability assessment was devised by Robert Fiedler and Hartmut Hetzler. The approach for checking regularity was devised by Hartmut Hetzler. Computational cost and convergence analysis were performed by Simon Bäuerle. The first draft of the manuscript was written by Robert Fiedler, Simon Bäuerle and Hartmut Hetzler and all authors commented on previous versions of the manuscript. All authors contributed to writing and revising the manuscript, and approved the final version.

Funding: Open Access funding enabled and organized by Projekt DEAL. The authors declare that no funds, grants, or other support were received during the preparation of this manuscript.

Availability of data, code and material: Data in this publication is available upon request. An open source MATLAB toolbox is under preparation and will be published on the website of the *Institute for Mechanics, Engineering Dynamics Group* (`www.uni-kassel.de/go/technische-dynamik`).

Declarations

Competing interest: The authors have no relevant financial or non-financial interests to disclose.

References

1. Argyris, J.H., Faust, G., Haase, M., Friedrich, R.: An Exploration of Dynamical Systems and Chaos. Springer, Berlin (2015)
2. Arnold, V.I., Neishtadt, A.I., Kozlov, V.V.: Mathematical aspects of classical and celestial mechanics. Encyclopaedia of Mathematical Sciences. Springer-Verlag, Berlin and Heidelberg, Germany (2006)
3. Bäuerle, S.: An Approach to Non-Linear Dynamics of Rotors with Flexible Seals: Models, Numerical Tools and Basic Phenomena. Ph.D thesis, Institute of Mechanics—Engineering Dynamics Group, University of Kassel, Kassel, Germany (2021)
4. Bäuerle, S., Fiedler, R., Hetzler, H.: An engineering perspective on the numerics of quasi-periodic oscillations. Nonlinear Dyn. (2022). https://doi.org/10.1007/s11071-022-07407-5
5. Benettin, G., Galgani, L., Giorgilli, A., Strelcyn, J.M.: Lyapunov characteristic exponents for smooth dynamical systems and for Hamiltonian systems; a method for computing all of them. Part 1: Theory. Meccanica **15**(1), 9–20 (1980)
6. Benettin, G., Galgani, L., Giorgilli, A., Strelcyn, J.M.: Lyapunov characteristic exponents for smooth dynamical systems and for Hamiltonian systems; a method for computing all of them. Part 2: Numerical application. Meccanica **15**(1), 21–30 (1980)
7. Broer, H.W., Hoo, J., Naudot, V.: Normal linear stability of quasi-periodic tori. J. Differ. Equ. **232**(2), 355–418 (2007)
8. Broer, H.W., Huitema, G.N., Sevryuk, M.B.: Quasi-Periodic Motions in Families of Dynamical Systems: Order Amidst Chaos. Springer, Berlin (1996)
9. Broer, H.W., Takens, F.: Dynamical Systems and Chaos. Springer, New York (2010)
10. Canadell, M., Haro, À.: Computation of quasiperiodic normally hyperbolic invariant tori: rigorous results. J. Nonlinear Sci. **27**(6), 1869–1904 (2017)
11. Chetayev, N.: The Stability of Motion [engl. transl. by M. Nadler]. Pergamon Press, New York (1961)
12. Choi, S.K., Noah, S.T.: Response and stability analysis of piecewise-linear oscillators under multi-forcing frequencies. Nonlinear Dyn. **3**(2), 105–121 (1992)
13. Christiansen, F., Rugh, H.H.: Computing Lyapunov spectra with continuous Gram–Schmidt orthonormalization. Nonlinearity **10**(5), 1063 (1997)
14. Dankowicz, H., Schilder, F.: Recipes for Continuation. SIAM, Philadelphia (2013)
15. Dieci, L., Russell, R.D., Van Vleck, E.S.: On the compuation of Lyapunov exponents for continuous dynamical systems. SIAM J. Numer. Anal. **34**(1), 402–423 (1997)
16. Doedel, E.J.: AUTO: a program for the automatic bifurcation analysis of autonomous systems. Congressus Numerantium **30**(265–284), 25–93 (1981)
17. Dormand, J.R., Prince, P.J.: A family of embedded Runge–Kutta formulae. J. Comput. Appl. Math. **6**(1), 19–26 (1980)
18. Fiedler, R.: Numerical analysis of invariant manifolds characterized by quasi-periodic oscillations of nonlinear systems. Dissertation, University of Kassel, Germany (2021)
19. Fontanela, F., Grolet, A., Salles, L., Hoffmann, N.: Computation of quasi-periodic localised vibrations in nonlinear cyclic and symmetric structures using harmonic balance methods. J. Sound Vib. **438**, 54–65 (2019)
20. Goldhirsch, I., Sulem, P.L., Orszag, S.A.: Stability and Lyapunov stability of dynamical systems: a differential approach and a numerical method. Physica D **27**(3), 311–337 (1987)
21. Gómez, G., Mondelo, J.M.: The dynamics around the collinear equilibrium points of the RTBP. Physica D **157**(4), 283–321 (2001)
22. Govaerts, W., Kuznetsov, Y.A., Dhooge, A., Mestrom, W., Am Riet, Sautois, B.: MATCONT and CL MATCONT: continuation toolboxes in Matlab. Tech. rep., Universiteit Gent, Belgium and Utrecht University, The Netherlands (2006)
23. Guskov, M., Thouverez, F.: Harmonic balance-based approach for quasi-periodic motions and stability analysis. J. Vib. Acoust. **134**(3) (2012)
24. Hahn, W.: Stability of Motion. Springer, Berlin (1967)
25. Henderson, M.E.: Flow box tiling methods for compact invariant manifolds. SIAM J. Appl. Dyn. Syst. **10**(3), 1154–1176 (2011)
26. Jorba, À.: Numerical computation of the normal behaviour of invariant curves of n-dimensional maps. Nonlinearity **14**(5), 943–976 (2001)
27. Kaas-Petersen, C.: Computation of quasi-periodic solutions of forced dissipative systems. J. Comput. Phys. **58**(3), 395–408 (1985)
28. Kaas-Petersen, C.: Computation of quasi-periodic solutions of forced dissipative systems II. J. Comput. Phys. **64**(2), 433–442 (1986)
29. Kaas-Petersen, C.: Computation, continuation, and bifurcation of torus solutions for dissipative maps and ordinary differential equations. Physica D **25**(1–3), 288–306 (1987)
30. Kim, Y.B., Noah, S.T.: Quasi-periodic response and stability analysis for a non-linear Jeffcott rotor. J. Sound Vib. **190**(2), 239–253 (1996)
31. Kuehn, C.: Multiple Time Scale Dynamics. Springer, Cham (2015)
32. Leonov, G.A., Kuznetsov, N.: Time-varying linearization and the Perron effects. Int. J. Bifurc. Chaos **17**(4), 1079–1107 (2007)
33. Liao, H., Zhao, Q., Fang, D.: The continuation and stability analysis methods for quasi-periodic solutions of nonlinear systems. Nonlinear Dyn. **100**(2), 1469–1496 (2020)
34. Lyapunov, A.M.: The general problem of the stability of motion [engl. transl. by a.t. fuller]. Int. J. Control **55**(3), 531–773 (1992)
35. Malkin, I.: Theory of Stability of Motion. United States Atomic Energy Commission, Oak Ridge, TN, USA (1952)

36. McCarthy, B.P., Howell, K.C.: Leveraging quasi-periodic orbits for trajectory design in cislunar space. Astrodynamics **5**(2), 139–165 (2021)
37. Olikara, Z.P., Scheeres, D.J.: Numerical method for computing quasi-periodic orbits and their stability in the restricted three-body problem. Adv. Astronaut. Sci. **145**(911–930) (2012)
38. Oseledec, V.I.: A multiplicative ergodic theorem: the Lyapunov characteristic numbers of dynamical systems. Trans. Moscow Math. Soc. **19**, 197–231 (1968)
39. Perron, O.: The question of stability in differential equations [in German]. Math. Z. **32**(1), 703–728 (1930)
40. Pikovsky, A., Rosenblum, M., Kurths, J.: Synchronization: A Universal Concept in Nonlinear Sciences. Cambridge Nonlinear Science Series, vol. 12. Cambridge University Press, Cambridge (2001)
41. Samoilenko, A.M.: Elements of the Mathematical Theory of Multi-frequency Oscillations. Springer, Dordrecht (1991)
42. Schilder, F., Osinga, H.M., Vogt, W.: Continuation of quasi-periodic invariant tori. SIAM J. Appl. Dyn. Syst. **4**(3), 459–488 (2005)
43. Schilder, F., Peckham, B.B.: Computing Arnol'd tongue scenarios. J. Comput. Phys. **220**(2), 932–951 (2007)
44. Schilder, F., Rübel, J., Starke, J., Osinga, H.M., Krauskopf, B., Inagaki, M.: Efficient computation of quasiperiodic oscillations in nonlinear systems with fast rotating parts. Nonlinear Dyn. **51**(4), 529–539 (2008)
45. Schilder, F., Vogt, W., Schreiber, S., Osinga, H.M.: Fourier methods for quasi-periodic oscillations. Int. J. Numer. Meth. Eng. **67**(5), 629–671 (2006)
46. Seydel, R.: Practical Bifurcation and Stability Analysis. Springer, New York (2010)
47. Shimada, I., Nagashima, T.: A numerical approach to ergodic problem of dissipative dynamical systems. Prog. Theor. Phys. **61**(6), 1605–1616 (1979)
48. Skokos, C.: The Lyapunov characteristic exponents and their computation. In: Dynamics of Small Solar System Bodies and Exoplanets, pp. 63–135. Springer, Berlin (2010)
49. Suarez, A., Fernandez, E., Ramirez, F., Sancho, S.: Stability and bifurcation analysis of self-oscillating quasi-periodic regimes. IEEE Trans. Microw. Theory Tech. **60**(3), 528–541 (2012)